EULER SOLUTIONS TO THE WAVY WALL PROBLEM

by

PHILIP PAUL BEAUCHAMP
M.S., University of Arizona, Tucson Az.
(1981)
B.S. Ae./Me., Syracuse University, Syracuse N.Y.
(1979)

Submitted to
the Department of Aeronautics and Astronautics
in Partial Fulfillment of the Requirements for
the Degree of

MASTER OF SCIENCE
IN AERONAUTICS AND ASTRONAUTICS

at the

MASSACHUSETTS INSTITUTE OF TECHNOLOGY
January, 1986

Signature of Author Signature redacted
Department of Aeronautics and Astronautics
January 15, 1986

Certified by Signature redacted
Professor Earll M. Murman
Thesis Supervisor

Accepted by Signature redacted
Professor Harold Y. Wachman, Chairman
Departmental Graduate Committee

EULER SOLUTIONS TO THE WAVY WALL PROBLEM

by

PHILIP PAUL BEAUCHAMP

Submitted to the Department of Aeronautics and Astronautics
on January 15, 1986 in partial fulfillment of the requirements for
the degree of Master of Science in Aeronautics and Astronautics.

ABSTRACT

A numerical solution to the classic wavy wall problem using the Euler equations has been explored. The solutions are obtained from a cell centered finite volume formulation using explicit time integration. Particular attention is paid to the formulation of consistent boundary conditions, and the solutions are made using at least three different boundary formulations. In addition to a boundary condition that is periodic in the flow direction, solutions are also made by enforcing the classical potential solution on all or part of the outer boundary and by solving a formulation consisting of one or more bumps in the flow direction. The latter formulation led to the discovery that specification of the downstream static pressure is not always the most consistent condition and can lead to convergence problems for some flows. This led to an investigation of the relative merits of using linearized characteristic boundary conditions with pressure specified at the outflow as oppossed to Riemann invariant boundary conditions.

In addition to the boundary condition comparison, results have been obtained for a number of different configurations covering subsonic, transonic, and supersonic flow. The comparison of the pressure outflow condition to the Riemann invariant condition demonstrates, that the Riemann invariant boundary condition is generally superior from a convergence standpoint. In addition, the pressure boundary condition leads to unacceptable transients for low Mach number flows. These transients are illustrated and discussed. The subsonic results demonstrate that periodic solutions can be obtained using either a series of bumps, a periodic boundary condition or by imposing the potential solution on the boundary. The latter solution is the most cost effective, but the periodic solution has the larger range of applicability. This is illustrated by computing a transonic result using a periodic boundary and comparing it to the multiple bump solution of the same problem. The difference in computation time for the two transonic solutions is found to be a factor of 25. Finally, it is demonstrated that, except for certain special cases, the supersonic problem can not be solved using the techniques presented. The inablility of the solver to perform these computations is traced to the boundary conditions, and illustrative examples are provided.

Thesis Supervisor: Dr. Earll M. Murman
Title: Professor of Aeronautics and Astronautics

ACKNOWLEDGEMENTS

I would like to thank Professor Earll Murman for his guidance and support through all the good and bad times that went into this study. His long hours and helpful suggestions were greatly appreciated. In addition, I would like to thank Professor Mike Giles for his enlightening discussions and comments.

I would also like to thank the members of the Computational Fluid Dynamics Lab, particularly Steve Allmaras and Ken Powell. It has been great fun and a real learning experience to work with all of you. I would also like to thank Bob Bruen for keeping the computer alive and kicking when I needed it most. Finally, I would like to thank my wife, Libbie, for staying by me through all the long hours, sleepless nights, and lost weekends.

This research was supported by my employer, the General Electric Company, to whom I am greatly indebted. In particular, I would like to thank Samir Sayegh, Dick Novak, and Dr. Roy Smith for their support while I attended MIT.

Contents

List of Figures

NOMENCLATURE

Variables:

A	Cell area.
$\tilde{A}$	Natural Euler operator.
$\ddot{A}$	Riemann Euler operator.
a	Sound speed.
$B(x,y)$	Wavy wall parametric equation
$\tilde{C}$	Linearized characteristic invariants.
$\ddot{C}$	Riemann characteristic invariants.
$D\{W\}$	Dissipation operator.
$\tilde{D}$	Intrinsic derivative along characteristics.
E	Energy per unit mass.
F	Numerical volume flux.
K	Transonic similarity parameter, $K = \frac{1-M_\infty^2}{\epsilon^{\frac{2}{3}} M_\infty}$.
I	Identity matrix.
M	Mach number.
m	Similarity parameter, $m = \sqrt{1-M_\infty^2}$.
$\aleph$	CFL number.
P	Pressure.
$P\{W\}$	Numerical flux operator.
$\vec{q}$	Velocity vector.
R	Radius of curvature.
$\Re$	Far field boundary functional.
$\tilde{S}$	Linearized similarity transformation.
$\ddot{S}$	Riemann similarity transformation.
t	time.
U	Free stream velocity.
u', v'	Perturbation velocities.
W	Conservation variables.
$\tilde{W}$	Natural primitive variables.
$\ddot{W}$	Riemann primitive variables.
x, y	Spatial coordinates.
X	x component of the flux vector.
Y	y component of the flux vector.
γ	Ratio of specific heats ; 1.4 for air.

δ, δ^3	Difference operators.
Δ	Increment or change.
ϵ	Wavy wall amplitude.
ε	Pressure Switch.
ς	Transformed space coordinate.
η	Transformed space coordinate, also, Surface normal vector.
Θ	Curvature.
κ^2, κ^4	Dissipation constants.
λ	Wavy wall wavelength. also, Characteristrics.
Λ	Characteristic matrix.
$\nu_{i,j}$	Normalized second difference of pressure.
ρ	Density.
σ	Control volume.
ϕ	Perturbation velocity potential.

Subscripts:

$body$	At the wall.
c	Corrected boundary value.
ff	Far field value.
i, j	Cell and node indices.
k	Face index.
p	Predicted interior boundary value.
η	Normal to grid boundaries.
ς	Tangential to grid boundaries.
$\mathfrak{F}$	Periodic face index.
∞	Freestream or reference state.

Superscripts:

n	Time step index.
$+$	Nondimensional.
$*$	Stage increment.
$\sim$	Linearized or Natural system.
$\cdot\cdot$	Riemann system.

Chapter 1

INTRODUCTION

The steady inviscid irrotational flow of a compressible fluid past a small amplitude sinusoidally varying wavy wall has been well explained using small perturbation theory[1][2]. For the subsonic and supersonic cases, the solutions are obtained by neglecting higher order terms in the perturbation equations. The resulting linearized perturbation potential equations can then be solved analytically[1]. For the case of transonic or hypersonic flow the small perturbation equations contain additional nonlinear terms which may not be neglected. In this case, the equations must be solved numerically. Chang and Kwon[3] have performed the calculation for transonic flows using the techniques originally developed by Murman and Cole[4] and subsequently expanded upon by others [5][6][7][8].

Solutions to the wavy wall problem obtained using the classic approximations are, as a consequence of Crocco's relation, isentropic. The validity of using this model to compute a transonic flow with shocks must be questioned. The transonic cases studied by Chang and Kwon result in shocks with a total pressure loss of at most 0.4 percent. Consequently, the isentropic flow assumption may be satisfactory for these cases. However, for flows with stronger shocks the Euler equations would clearly provide

a better model of the flow nonlinearities. Relaxation of the isentropic flow restrictions, however, introduces other issues which must be addressed.

For wavy walls with larger amplitudes or higher flow velocities, the shock strength may increase dramatically. The resulting entropy increase and total pressure loss would then be convected downstream. Any subsequent shocks would therefore be weakened by the aggregate total pressure loss of the preceding shock(s). Since this flow must have an intial shock followed by a series of weaker shocks, the implication is that the problem may no longer be a boundary value problem but rather it may be an initial value problem. Eventually the flow field *may* reach a condition where it is periodic in space, however, there is no guarantee that this is going to be the case. If the problem is truly an initial value problem, then it will not be possible to use periodic boundary conditions for computing the flow field.

The problem of interest is the time accurate computation of an inviscid compressible flow past a sinusoidally varying wall of arbitrary amplitude. The wall may or may not have a flat region upstream and downstream of the bumps, and the boundary condition to be applied may or may not be periodic. Since the solution can be highly nonlinear, the Euler equations must be solved numerically. Because time accuracy may be important, it will be judicious to choose a numerical algorithm which is time accurate. For the results presented herein, the finite volume technique developed by Jameson, Schmdit, and Turkel[9] has been used. Time accuracy was maintained by integrating with an explicit four stage Runge–Kutta scheme. The implementation is

such that the algorithm may be run using either a fixed CFL condition or a fixed time step. The fixed CFL condition allows for faster convergence of those solutions which have steady state solutions that do not have to be computed time accurately.

The solutions to be presented cover a wide variety of classic wavy wall and sine bump problems. For all three regimes of flow (subsonic, transonic, and supersonic) the problem has been solved as an initial value problem using multiple bumps. This problem is very similar to the Ni bump problem[10]. The main differences between the Ni problem and the one presented are the possibility of multiple bumps and the inclusion of a free upper boundary instead of a solid wall. For small amplitude waves both the subsonic and supersonic classic wavy wall problems were tried by imposing the small perturbation solution at the boundary of the computational domain. In addition, solutions in all three regimes were attempted using a formulation consisting of boundary conditions that were periodic in the flow direction.

During the course of the investigation it was discovered that the implementation of the boundary conditions seriously impacted on the flow computation. Numerous implementations of the boundary conditions were tried with varying degrees of success. As mentioned previously the problem was attempted using three formulations, (periodic, imposed potential, and multiple bump). In each case there is at least one boundary which may be considered free or open. Along these bounadaries the boundary conditions were implemented using both linearized invariant and Riemann invariant formulations. Because the solutions for the multiple bump flows were expected to be computationally

expensive an investigation into the relative merit of the two approaches was undertaken. Using a Ni bump type formulation, a single sine bump along a flat wall with a free top boundary was examined in both subsonic and transonic flow using both the linearized and Riemann invariants.

The results of the comparison between the linearized invariant and Riemann invariant boundary conditions provided some surprises. The expected result that the Riemann conditions generally lead to faster convergence was verified. The unexpected result was that for low Mach number flows the linearized boundary conditions resulted in a transient phenomena that prevented convergence. The reasons for this are not conclusive and more research is required in this area. However, based on observations of the solution details, some conjectures will be put forth.

The results of the numerical evaluations of the subsonic wavy wall problem show that the Euler flow appears to be periodic and that it may be obtained using any of the formulations described. It is found that the multiple bump method is the most expensive and the imposed potential method is the least expensive.

The transonic problem can be solved either as a multiple bump problem or as a periodic problem. In this case it is found that the problem is best described as an initial value problem. The solution consists of a series of shocks that become progressively weaker as the fluid flows over each successive wave crest. The weakening process continues until the flow reaches a condition where the stagnation pressure loss is sufficiently high enough to result in waves with a single sonic point. From this point on the solution

appears to be periodic in space.

The supersonic results show that unless very specific criteria are met the problem can not be solved using the boundary conditions outlined above. In particular, it will be shown that both the linearized and Riemann invariant boundary conditions reflect waves incident on the outflow boundary unless the far field information provided to the boundary conditions correctly sets the two dimensional supersonic characteristics.

Chapter 2

THE POTENTIAL WAVY WALL

The wavy wall problem is the classic example of an application of the linearized small perturbation equations to the solution of a fluid flow problem. To provide an adequate base from which to consider the Euler solution to the same problem, it will be instructive to first outline this solution. The first step will be to state the linearized small perturbation equations and their associated boundary conditions. The solution for subsonic flow over a sinusoidally varying wavy wall will then be presented. This will be followed by the solution for the supersonic case. Finally, the non-linear transonic case, will be discussed.

2.1 Small Perturbation Equations

Consider a flow field where the velocity, $\vec{q}$, may be represented as the sum of a uniform far field velocity and a small perturbation to that field. In two dimensions, for a uniform far field flow in the x direction, this statement takes the form

$$q_1 = U + u' \tag{2.1a}$$

$$q_2 = v' \tag{2.1b}$$

Here, u' and v' are the peturbation velocities and U is the uniform far field velocity. These velocities may be substituted into the equations of motion for the steady, inviscid, isentropic, flow of a compressible fluid [1],

$$q_i q_j \frac{\partial q_i}{\partial x_j} = a^2 \frac{\partial q_k}{\partial x_k}. \tag{2.2}$$

Here a^2 is the square of the local speed of sound which is obtained from the energy equation for a perfect gas,

$$a^2 = a_\infty^2 - \frac{\gamma - 1}{2}(2u'U + u'^2 + v'^2). \tag{2.3}$$

Perfoming the indicated substitutions and neglecting small terms, yields the two–dimensional small perturbation equation,

$$(1 - M_\infty^2)\frac{\partial u'}{\partial x} + \frac{\partial v'}{\partial y} = M_\infty^2(\gamma + 1)\frac{u'}{U}\frac{\partial u'}{\partial x}. \tag{2.4}$$

As developed, equation (2.4) is valid for subsonic, transonic, and supersonic flow. By restricting the fields of interest to those which are either subsonic or supersonic the terms on the right hand side can be dropped. The result is the classic small perturbation equation.

$$(1 - M_\infty^2)\frac{\partial u'}{\partial x} + \frac{\partial v'}{\partial y} = 0 \tag{2.5}$$

Introducing the additional assumption that the flow field is irrotational, implies that a velocity potential, ϕ, exists and may be defined,

$$u' \equiv \frac{\partial \phi}{\partial x}, \qquad v' \equiv \frac{\partial \phi}{\partial y}. \tag{2.6}$$

Substituting equations (2.6) into the small perturbation equation (2.6) yields a result for the perturbation potential,

$$(1 - M_\infty^2)\frac{\partial^2 \phi}{\partial x^2} + \frac{\partial^2 \phi}{\partial y^2} = 0. \tag{2.7}$$

The result is a second order linear partial differential equation whose type is dependent on the sign of the leading coefficient. For subsonic flow the equation is elliptic and is easily solved by separation of variables. For supersonic flow the equation reduces to a simple wave equation (hyperbolic type) and is solved by characteristic methods.

2.2 Perturbation Boundary Conditions

The solution of the governing equation for some arbitrary flow field and geometry requires that certain boundary conditions be specified. In particular, it is necessary to specify a condition for all solid boundaries as well as a far field condition. The condition at impermeable boundaries ensures that flow does not pass through that boundary. The far field condition generally takes the form of a restriction on unbounded growth of the perturbations. These conditions are detailed below.

2.2.1 Solid Boundary Condition

At the surface of an impermeable solid boundary it will be necessary to impose the so called *tangency condition*. This states that at the solid surfaces the velocity vector must be at right angles to the surface normal vector. If the geometry of the surface is

described by the parametric equation,

$$B(x, y) = 0, \tag{2.8}$$

then the boundary condition takes the form,

$$\vec{q} \cdot \nabla B(x, y) = 0. \tag{2.9}$$

Introducing the perturbation velocities from equations (2.1) into the above result yields

$$(U + u')\frac{\partial B(x, y)}{\partial x} + v'\frac{\partial B(x, y)}{\partial y} = 0. \tag{2.10}$$

Recalling that the perturbation velocity is much smaller than the far field velocity, $u' \ll U$, it is possible to neglect the term involving u'. If this can be done, then the boundary condition at a solid wall can be approximated by

$$U\frac{\partial B(x, y)}{\partial x} + v'\frac{\partial B(x, y)}{\partial y} = 0. \tag{2.11}$$

This result may be rearranged to show that on the body

$$v'(x, y)_{body} = U\left(\frac{dy}{dx}\right)_{body}. \tag{2.12}$$

If the flow field contains purely small perturbations, one further simplification can be made. It is clear that the geometry must consist of small deviations from some neutral locus. This implies that the geometry must be thin and that it deviates very little from $y = 0$. Within the framework of small perturbation theory the boundary condition can therefore be imposed at $y = 0$, where it becomes

$$v'(x, 0) = U\left(\frac{dy}{dx}\right)_{body}. \tag{2.13}$$

Finally, recall the definition of the perturbation potential given by equation (2.6). Substituting into eqaution (2.13) it can seen that

$$\frac{\partial \phi(x,0)}{\partial y} \equiv v'(x,0) = U \left(\frac{dy}{dx}\right)_{body} \tag{2.14}$$

is the solid surface boundary condition for the perturbation potential equation.

2.2.2 Far Field Condition

In addition to applying the flow tangency condition at solid surfaces, it will be necessary to say something about the nature of the flow at the far field. The exact nature of this specification is problem dependent. It generally takes the form of a statement that at the far field the velocity perturbations are either zero or finite. A mathematical statement of this condition would take the form

$$\frac{\partial \phi(x_{ff}, y_{ff})}{\partial x} = \Re_1 \tag{2.15a}$$

$$\frac{\partial \phi(x_{ff}, y_{ff})}{\partial y} = \Re_2 \tag{2.15b}$$

where $\Re_1$ and $\Re_2$ are finite and the subscript ff indicates the far field location. The parameters, $\Re_1$ and $\Re_2$ may be constant or they may be functions of x_{ff} and/or y_{ff}.

2.3 Flow Past a Wavy Wall

Consider the flow past a sinusoidally varying wall, such as the one shown in Figure 2.1. The boundary equation for this wall takes the form

$$y = \epsilon \sin\left(\frac{2\pi x}{\lambda}\right), \tag{2.16}$$

where ϵ is the *amplitude* of the wall bump, and λ is its *wavelength.*

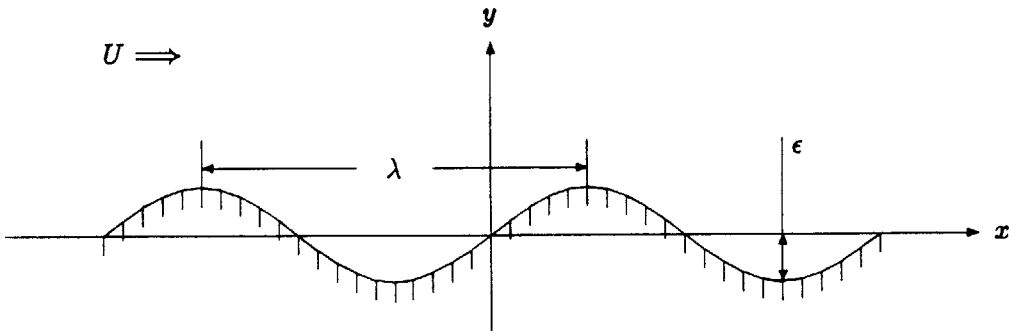

Figure 2.1: A Sinusoidally Varying Wavy Wall

For either subsonic or supersonic flow the solution may be found by solving equation (2.7) subject to the boundary conditions that,

$$\frac{\partial \phi(x,\infty)}{\partial x} \quad , \quad \frac{\partial \phi(x,\infty)}{\partial y} \quad \text{are bounded} \tag{2.17}$$

and along the wall, $y = 0$,

$$\frac{\partial \phi(x,0)}{\partial y} = \frac{U\epsilon 2\pi}{\lambda} \cos\left(\frac{2\pi x}{\lambda}\right). \tag{2.18}$$

The latter is a statement of the flow tangency condition derived from equations (2.14) and (2.16). The first condition ensures that the peturbation velocities do not grow at large distances from the wall.

2.3.1 Subsonic Wavy Wall Solution

Start by considering flow over the wavy wall when the free stream Mach number is subsonic, and there is no transonic flow at any point along the wall. For this flow $m^2 \equiv 1 - M_\infty^2$ is greater than zero and the governing equation, (2.7), is clearly elliptic in nature. The solution is obtained by rewriting the equation as,

$$\frac{\partial^2 \phi}{\partial x^2} + \frac{1}{m^2}\frac{\partial^2 \phi}{\partial y^2} = 0, \tag{2.19}$$

and then looking for a solution of the form,

$$\phi(x, y) = P(x)Q(y). \tag{2.20}$$

Substituting the assumed solution into the governing partial differential equation yields

$$\frac{1}{P}P'' + \frac{1}{m^2 Q}Q'' = 0. \tag{2.21}$$

The first term of this result is a function of x alone while the second term is strictly a function of y. The equation is therefore separable, and may be written as the system,

$$\frac{1}{P}P'' = -k^2 \tag{2.22a}$$

$$\frac{1}{m^2 Q}Q'' = k^2 \tag{2.22b}$$

where k is a real constant. The general solution to these equations is given by,

$$P(x) = c_1 \sin(kx) + c_2 \cos(kx) \tag{2.23a}$$

$$Q(y) = c_3 e^{-mky} + c_4 e^{mky}. \tag{2.23b}$$

Application of the far field boundary condition, equation (2.17), implies that $c_4 = 0$. The boundary condition along the wall, equation (2.18) can be easily satified by selecting $c_1 = 0$ and $k = \frac{2\pi}{\lambda}$ with

$$c_2 c_3 = \frac{U\epsilon 2\pi}{\lambda mk}. \tag{2.24}$$

Collecting the various terms and substituting into equation (2.20) the perturbation potential is found to be

$$\phi(x,y) = \frac{-U\epsilon \cos\left(x\frac{2\pi}{\lambda}\right)}{\sqrt{1-M_\infty^2}} \left\{ e^{-y\frac{2\pi}{\lambda}\sqrt{1-M_\infty^2}} \right\}. \tag{2.25}$$

The velocity at any point in the field is found by combining equations (2.1) and (2.6) with the result just determined. The resulting field is then given by

$$q_1(x,y) = U + \frac{U\epsilon 2\pi \sin\left(x\frac{2\pi}{\lambda}\right)}{\lambda\sqrt{1-M_\infty^2}} \left\{ e^{-y\frac{2\pi}{\lambda}\sqrt{1-M_\infty^2}} \right\} \tag{2.26}$$

$$q_2(x,y) = \frac{-U\epsilon 2\pi \cos\left(x\frac{2\pi}{\lambda}\right)}{\lambda} \left\{ e^{-y\frac{2\pi}{\lambda}\sqrt{1-M_\infty^2}} \right\}. \tag{2.27}$$

The solution for the subsonic flow case indicates that the largest perturbations occur near the wall. The magnitude of the perturbations decays exponentially above the wall and the perturbations are periodic in the x direction. The exponential decay away from the wall is attenuated by the factor $\sqrt{1-M_\infty^2}$ so, as the Mach number increases, the attenuation becomes slower. An example of the solution is shown in Figure 2.2.

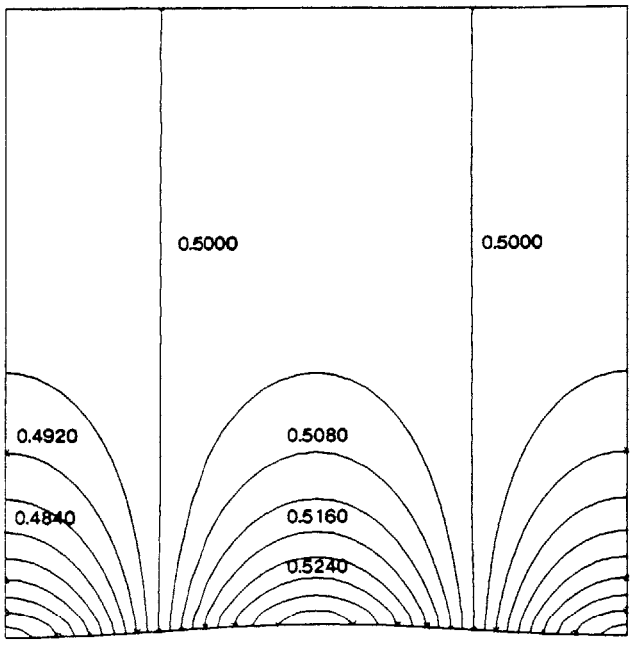

Figure 2.2: Subsonic Flow, $M = 0.5$, Over a Wavy Wall, $\epsilon = 0.01$

2.3.2 Supersonic Wavy Wall Solution

Consider now the case in which the flow over the wavy wall occurs at supersonic velocities. For this case, $m^2 \equiv 1 - M_\infty^2$ is less than zero so that the governing equation is now hyperbolic. Introducing the change of variables $\Lambda^2 \equiv -m^2 = M_\infty^2 - 1$, the governing equation may be written as

$$\frac{\partial^2 \phi}{\partial x^2} - \frac{1}{\Lambda^2} \frac{\partial^2 \phi}{\partial y^2} = 0. \tag{2.28}$$

This equation is a simple wave equation, which can be solved by looking for a solution of the form,

$$\phi(x, y) = F(x - \Lambda y) + G(x + \Lambda y). \tag{2.29}$$

The boundary conditions are identical to those given for the subsonic case, equations (2.17) and (2.18).

The solution proposed above is characteristic in nature. Along the lines $x - \Lambda y$, the solution has $F = \text{const.}$, and along the lines $x + \Lambda y$, the solution has $G = \text{const.}$. Considering only the upper half plane for left to right flow, it is clear that the funtion F holds along downstream inclined characteristics that *originate* at the wall. On the other hand, the function G holds along the upstream running characteristics that *originate* at infinity. To prevent the influence of the wall from progating upstream in a supersonic flow, a physical impossibility, it is necessary that the function G be identically zero. Therefore, the solution is of the form

$$\phi(x, y) = F(x - \Lambda y) \tag{2.30}$$

Substituting this form of the solution into the equation for the solid wall boundary condition, equation (2.18) it is seen that

$$\Lambda F'(x) = -\frac{U\epsilon 2\pi}{\lambda} \cos\left(\frac{2\pi x}{\lambda}\right). \tag{2.31}$$

Here F' denotes the derivative of F with respect to $x - \Lambda y$. Integrating this result, and noting that constant can be set to zero with no loss of generality, the solution becomes,

$$F(x) = -\frac{U\epsilon}{\Lambda} \sin\left(\frac{2\pi x}{\lambda}\right), \tag{2.32}$$

and thus the perturbation potential is

$$\phi(x, y) = -\frac{U\epsilon}{\sqrt{M_\infty^2 - 1}} \sin\left(\frac{2\pi}{\lambda}\left[x - y\sqrt{M_\infty^2 - 1}\right]\right). \tag{2.33}$$

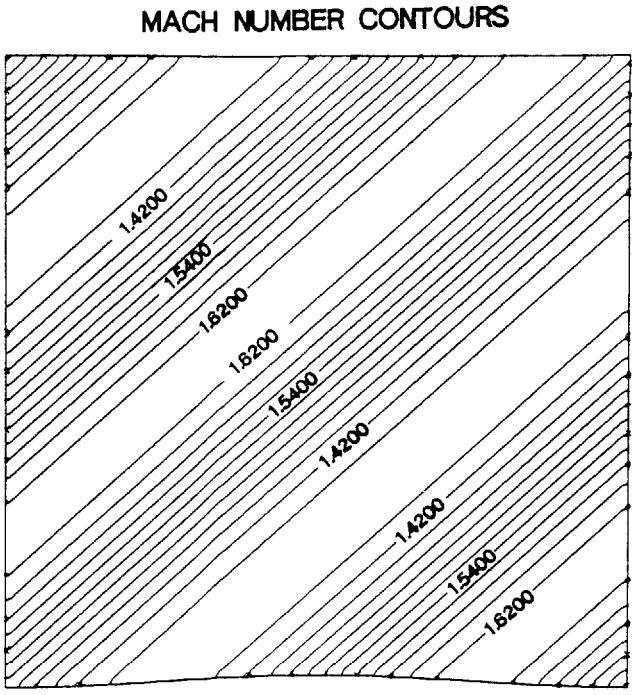

Figure 2.3: Supersonic Flow, $M = 1.5$, Over a Wavy Wall, $\epsilon = 0.01$

As before, the velocity at any point in the field can be determined from equations (2.1) and (2.6). For the supersonic case the result takes the form

$$q_1(x,y) = U - \frac{U\epsilon 2\pi}{\lambda\sqrt{M_\infty^2 - 1}} \cos\left(\frac{2\pi}{\lambda}\left[x - y\sqrt{M_\infty^2 - 1}\right]\right) \tag{2.34}$$

$$q_2(x,y) = \frac{U\epsilon 2\pi}{\lambda} \cos\left(\frac{2\pi}{\lambda}\left[x - y\sqrt{M_\infty^2 - 1}\right]\right). \tag{2.35}$$

The solution for the supersonic case, like the subsonic case, is periodic in the x direction. Unlike the subsonic case, however, the supersonic solution contains no exponential decay. Instead the perturbations are constant along the characteristic lines. This case is an example of a far field which is finite but periodic in x. An example of this flow is shown in Figure 2.3.

2.3.3 Transonic Wavy Wall Solutions

Finally, consider the case of flow over the wavy wall when the free steam Mach number is sufficiently high to allow the field to accelerate through the sonic conditions over a portion of the boundary. For this transonic flow, it is necessary to retain the nonlinear terms on the right hand side of equation (2.4). Consequently, there is no simple analytical solution for this case. The problem can be solved numerically, and such a computation has been performed by Chang and Kwon [3].

The computations by Chang and Kwon are reported in terms of the transonic similarity parameter,

$$K = \frac{1 - M_\infty^2}{\epsilon^{\frac{2}{3}} M_\infty} \quad . \tag{2.36}$$

The parameter is such that the value $K = 0$ represents the boundary between subsonic and supersonic free stream Mach numbers. By performing numerical experiments the authors found that the flow becomes supercritical for transonic similarity parameters of $K \leq 7.03$. The computed results indicate that solutions to equation (2.4) are periodic in the x direction. For flow fields in which $0 < K \leq 7.3$ (the transonic regime) the results consist of a subsonic flow field with an embedded supersonic region which generally terminates in a shock. At the value of $K = 0$ there a pure sonic point on the crest of the wave. As the free stream Mach number is increased (K dropping) the sonic point moves forward on the wave and a terminating shock occurs on the rearward face. As the value of K is dropped further the shock strengthens and moves further aft of the wave crest.

Chapter 3

EULER FORMULATION

The formulation of the wavy wall problem assuming two-dimensional, inviscid compressible fluid flow is somewhat different than that for potential flow. In particular, the governing equations must allow for solutions which may be unsteady and which may have entropy generation. The governing Euler equations for such flows will be summarized below. The non–dimensional form of the governing equations will be outlined. Finally, the physical boundary conditions will be developed.

3.1 2–D Euler Equations

The flow of a compressible inviscid fluid is governed by the Euler equations. For a two–dimensional flow, if we let ρ, u, v, P, and E denote the density, Cartesian velocity components, pressure and energy per unit mass, then for a perfect gas the equation of state becomes

$$E = \frac{P}{\rho(\gamma - 1)} + \frac{u^2 + v^2}{2} \tag{3.1}$$

where γ is the ratio of the specific heats. The unsteady Euler equations, representing

conservation of mass, momentum, and energy, may then be written in integral form as

$$\frac{\partial}{\partial t}\iint_{\sigma} W\,dx\,dy + \oint_{\partial\sigma}(X\,dy - Y\,dx) = 0, \tag{3.2}$$

where the integral is evaluated over the control volume σ bounded by the closed curve $\partial\sigma$. The conservation variables W and the flux quantities, X and Y, are given by the relations

$$W = \begin{Bmatrix} \rho \\ \rho u \\ \rho v \\ \rho E \end{Bmatrix}, \quad X = \begin{Bmatrix} \rho u \\ \rho u^2 + P \\ \rho uv \\ \rho Eu + Pu \end{Bmatrix}, \quad Y = \begin{Bmatrix} \rho v \\ \rho uv \\ \rho v^2 + P \\ \rho Ev + Pv \end{Bmatrix}. \tag{3.3}$$

If steady state solutions to these equations are desired, it is possible to reduce the system to a three equation model. This is done by noting that in the steady state, the total enthalpy is constant. The system can then be reduced to the isoenergetic Euler equations [11]. For the wavy wall flows under consideration it is not clear that the solutions will be steady. For this reason, the complete system of equations obtained above will be retained and the four equation model will be used throughout.

3.2 Nondimensionalization

To simplify the implementation of the numerical algorithm, it is recommended that the governing equations be nondimensionalized. The effect of the transformation is transparent to the governing equations while, at the same time, it simplifies the boundary conditions. Since the form of the Euler equations does not change under the transformation, any choice of consistent nondimensional parameters may be used.

In the algorithm developed below, the flow variables have been nondimensionalized by the far field static density and velocity. For the purposes of this report, the far field is defined as the region $y = +\infty$. In addition, the Cartesian coordinates have been nondimensionalized to obtain a unit wavelength for the wall. Denoting nondimensional values by $()^+$, and denoting the far field quantities by $()_{ff}$ the flow variables become

$$\begin{aligned} u^+ &= \frac{u}{u_{ff}} \qquad v^+ = \frac{v}{u_{ff}} \\ P^+ &= \frac{P}{\rho_{ff} u_{ff}^2} \quad \rho^+ = \frac{\rho}{\rho_{ff}} \quad E^+ = \frac{E}{u_{ff}^2} \end{aligned} \tag{3.4}$$

From this point on however, the superscript notation will be dropped and all quantities will be interpreted as being nondimensional.

3.3 Boundary Conditions

The Euler equations alone are insufficient to uniquely determine a fluid flow field. It is necessary to close the system by introducing appropriate boundary conditions. The boundary condition formulation developed below is purely analytic. The specific details for a wavy wall and the implemention of the boundary conditions in the numerical algorithm will be discussed later.

3.3.1 Solid Boundary Condition

Looking first at the physical boundary conditions, note that solid surfaces will be considered impermeable. If the fluid velocity vector is $\vec{q}$ and the outward unit normal vector to the surface is $\vec{\eta}$, then the no flux condition is simply

$$\rho \vec{q} \cdot \vec{\eta} = 0. \tag{3.5}$$

If the Euler equations are written in natural coordinates,

$$\frac{\partial}{\partial t}\iint_{\sigma}\begin{Bmatrix}\rho\\ \rho u\\ \rho v\\ \rho E\end{Bmatrix}dx\,dy+\oint_{\partial\sigma}\begin{Bmatrix}\rho\vec{q}\cdot\vec{\eta}\\ \rho\vec{q}\cdot\vec{\eta}u+P\eta_x\\ \rho\vec{q}\cdot\vec{\eta}v+P\eta_y\\ \rho\vec{q}\cdot\vec{\eta}(E+\frac{P}{\rho})\end{Bmatrix}ds=0, \tag{3.6}$$

then from equation (3.5) it is clear that the no mass flow condition eliminates all wall fluxes except the pressure flux in the two momentum equations.

3.3.2 Far Field Condition

A unique solution to the Euler equations requires the specification of a far field condition. The usual approach is to specify the free stream flow condition. This condition should be specified at an infinite distance from the body. From a practical point of view, this boundary condition is of no use in a numerical algorithm where the computational boundary does not occur at infinity. Thus, the numerical scheme generally employs some other boundary condition at the edge of the domain. For the algorithm used herein a number of different numerical boundary conditions have been tried. A complete derivation of each will be presented after the interior algorithm is described.

Chapter 4

INTERIOR NUMERICAL ALGORITHM

Determination of the flow field over a wavy wall using the Euler equations requires the development of a discrete approximation to the governing equations. The discretized system must then be integrated in time to determine the solution. In this work, the finite volume multistage scheme developed by Jameson, Schmidt, and Turkel[9] has been used. This method has the advantage of being able to accurately march forward in time. The spatial discretization and time marching techniques are outlined below along with a discussion of the grids used. Because it was found that the boundary conditions had a large impact on solution convergence, the discussion of their implementation will be deferred.

4.1 Finite Volume Formulation

The multistage scheme developed by Jameson, Schmidt, and Turkel assumes a solution that is spatially discrete. This discrete approximation to the spatial derivatives yields a large coupled set of ordinary differential equations which are integrated in time using a Runge–Kutta formulation. By fixing the time step it is possible, if certain criteria are met, to accurately march forward in time. It is also possible, under the

assumption that there is a steady state solution, to march forward at an accelerated rate to an asymptotic time-invariant state.

4.1.1 Grid Generation

The problems to be considered herein are such that the displacement of the elevated or wavy region of the solid wall is a sine wave of the form

$$y = \epsilon \sin(2\pi x), \tag{4.1}$$

where it has been assumed that the wavelength, λ, is 1. The problems considered, however, are not restricted to the classical wavy wall problem which is infinite in x. Thus, some of the solutions consist of one or more sinusoidal bumps with a flat upstream and downstream region.

Solutions to the Euler equation are to be found in a rectangular region surrounding the wave(s), see Figure 4.1. Since application of the solid wall boundary conditions is simplified for an orthogonal grid, the following grid generation technique has been used. For a given rectangular region, the upper constant y surface and the lower solid boundary surface are defined such that the points in the x direction have a constant Δx. The inflow and outflow boundary points are defined at constant x locations with the y points distributed using an exponential stretch.

It is then assumed that in some transformed space, (ς, η), the grid satisfies the Laplacians

$$\frac{\partial^2 y}{\partial \varsigma^2} + \frac{\partial^2 y}{\partial \eta^2} = 0 \tag{4.2a}$$

$$\frac{\partial^2 x}{\partial \zeta^2} + \frac{\partial^2 x}{\partial \eta^2} = 0. \tag{4.2b}$$

The grid is developed by first solving equation (4.2a) for the y coordinates interior to the domain. This is done by applying a straight forward Gauss-Seidel technique, with $\Delta\zeta = \Delta\eta = 1$,

$$y_{i,j}^{n+1} = 0.25(y_{i-1,j}^{n+1} + y_{i,j-1}^{n+1} + y_{i+1,j}^{n} + y_{i,j+1}^{n}) \tag{4.3}$$

to an initial grid obtained by scaling the y coordinates at each x location to those at the inflow.

The solution for the x coordinates could be found by developing an equation similar to that for the y direction. Unfortunately, this would result in a series of constant x lines that would not be orthogonal to the lines found previously. This occurs because the system (4.2), does not necessarily imply that the Cauchy–Riemann condition

$$\frac{\partial x}{\partial \eta} = -\frac{\partial y}{\partial \zeta} \quad , \quad \frac{\partial x}{\partial \zeta} = \frac{\partial y}{\partial \eta} \tag{4.4}$$

is satisfied. This condition is enforced by first writing equation (4.2b) as

$$x_{i,j}^{n+1} = 0.25(x_{i-1,j}^{n+1} + x_{i,j-1}^{n+1} + x_{i+1,j}^{n} + x_{i,j+1}^{n+1}). \tag{4.5}$$

Recalling that the the y points have already been fixed, the Cauchy–Riemann condition then becomes,

$$x_{i,j+1}^{n+1} = x_{i,j-1}^{n+1} - (y_{i+1,j} - y_{i-1,j}). \tag{4.6}$$

Substituting this result into equation (4.5) yields the grid generation scheme for the x points,

$$x_{i,j}^{n+1} = 0.25(x_{i-1,j}^{n+1} + 2x_{i,j-1}^{n+1} + x_{i+1,j}^{n} - y_{i+1,j} + y_{i-1,j}). \tag{4.7}$$

It is worth noting that the imposition of the first of equations (4.4) in (4.2b), guarantees that the second equation is satisfied to within a constant, which is set to zero by selecting a rectangular transform space.

Grid generation using the technique implied by equations (4.3) and (4.7) works well as long has the wave amplitude is not too high. The method is easy to code, converges rapidly, and because it does not use the node $j+1$, it can be used to automatically redistribute the x points along the upper surface. For cases where the wave amplitude is too large the method can be modified to solve the two equations simultaneously. Examples of the grids obtained using this technique are shown in Figure 4.2.

4.1.2 Spatial Discretization

To visualize the spatial discretization, consider some representative cell within the grid, Figure 4.3. The coordinates are stored at the cell nodes while the conservation variables, W in equation (3.3), are stored at the cell centers. Assuming the conservation variables are constant over the cell, then for each cell in the domain equation (3.2) may be replaced by the system

$$\frac{\partial}{\partial t} A \begin{Bmatrix} \rho \\ \rho u \\ \rho v \\ \rho E \end{Bmatrix} + \sum_{k=1}^{4} \begin{Bmatrix} F_k \rho_k \\ F_k(\rho u)_k + \Delta y_k P_k \\ F_k(\rho v)_k - \Delta x_k P_k \\ F_k(\rho E)_k + F_k P_k \end{Bmatrix} = 0. \tag{4.8}$$

Here, A is the cell area, and k is the subscript for the cell face. In addition, F_k is the

volume flux of the k^{th} cell face, which is given by

$$F_k = \Delta y_k u_k - \Delta x_k v_k. \tag{4.9}$$

The values of the conservation quantities at each face in equation (4.8) are obtained by averaging the values of the appropriate conservation variables on either side of the face. The value for the pressure is obtained by averaging the two pressures implied by the conservation variables on either side of the face. It is clear from equation (4.8) that the scheme is conservative and should, therefore, correctly predict the shock location and jump relations.

4.1.3 Artificial Dissipation

The finite difference scheme outlined above is equivalent, on a Cartesian grid, to a second order central difference scheme. Unfortunately, this makes the technique susceptible to odd–even decoupling. It is therefore necessary to add artificial viscosity to the scheme.

To reduce the occurence of odd–even decoupling a fourth difference smoothing operator is applied to each cell. In addition, a second difference smoothing operator is used to smear the shocks over a few cells, thereby allowing the algorithm to properly capture the shocks. This treatment at the shocks retains the correct shock jump relations[12].

The discrete approximation for the Euler system, equation (4.8), may be written in the alternative form,

$$\frac{d}{dt}\{AW\} + P\{W\} = 0. \tag{4.10}$$

Here $P\{W\}$ is the operator,

$$P\{W\} = \sum_{k=1}^{4} \begin{Bmatrix} F_k \rho_k \\ F_k(\rho u)_k + \Delta y_k P_k \\ F_k(\rho v)_k - \Delta x_k P_k \\ F_k(\rho E)_k + F_k P_k \end{Bmatrix}. \tag{4.11}$$

Dissipation is added to the scheme by modifying equation (4.11) to be of the form,

$$P\{W\} = \sum_{k=1}^{4} \begin{Bmatrix} F_k \rho_k \\ F_k(\rho u)_k + \Delta y_k P_k \\ F_k(\rho v)_k - \Delta x_k P_k \\ F_k(\rho E)_k + F_k P_k \end{Bmatrix} - D\{W\}, \tag{4.12}$$

where $D\{W\}$ is the dissipation operator which is a blend of second and fourth differences.

The dissipation operator used for this work closely follows the development given by Jameson, Schmidt, Turkel[9]. The operator may be written as

$$D\{W\} = \sum_{k=1}^{4} \left(\frac{A}{\Delta t}\right) [\varepsilon_k^{(2)} \delta_k\{W\} - \varepsilon_k^{(4)} \delta_k^3\{W\}], \tag{4.13}$$

where the difference operators, $\delta_k\{W\}$ and $\delta_k^3\{W\}$, are, for the face $k = 2$, of the form

$$\delta_k\{W\} = W_{i+1,j} - W_{i,j} \tag{4.14a}$$

$$\delta_k^3\{W\} = W_{i+2,j} - 3W_{i+1,j} + 3W_{i,j} - W_{i-1,j}. \tag{4.14b}$$

The second difference pressure switch, $\varepsilon_k^{(2)}$, at the face $(i + \frac{1}{2}, j)$ is given by

$$\varepsilon_k^{(2)} = \kappa^2 \quad \text{MAX}\{\nu_{i+1,j} \ , \ \nu_{i,j}\} \tag{4.15}$$

with similar representations for the other faces. Here ν is defined for each cell as

$$\nu_{i,j} = \left| \frac{P_{i+1,j} - 2P_{i,j} + P_{i-1,j}}{P_{i+1,j} + 2P_{i,j} + P_{i-1,j}} \right| . \tag{4.16}$$

The fourth difference pressure switch is of the form

$$\varepsilon_k^{(4)} = \text{MAX}\{0, \kappa^4 - \varepsilon_k^{(2)}\} \tag{4.17}$$

and is defined so the second and fourth difference operators are mutually exclusive.

The constants κ^2 and κ^4 are user input parameters that set the dissipation level. The constant κ^2 controls the smearing of shocks. For the solutions reported here it has been set to $\kappa^2 = 0.25$ for all fields characterized by supersonic flow. For all subsonic cases it has been set to zero. The constant κ^4 adjusts the background dissipation level for the scheme. A value of $\kappa^4 = 0.0075$ has been used for the results reported.

At the boundaries of the domain, the dissipation scheme must be modified to maintain global consevation. Eriksson[13] has shown that setting the dissipation flux on a boundary face to zero, results in a globally dissipative smoothing operator that is also globally conservative. The algorithm used herein uses this approach in applying the artificial viscosity.

4.2 Time Integration Schemes

Applying the spatial discretization to each cell in the domain results in a large system of coupled ordinary differential equations which are to be marched forward in time. If a time accurate solution to the problem is desired, it will be necessary to march

in time using a fixed Δt at each cell. The Δt so choosen must be governed by the Δt for the most restrictive cell in the domain. This can lead to rather lengthy computation times but it is unavoidable for time accurate solutions using an explicit method. On the other hand, if only the steady state solution is desired, then it is possible to march using the maximum allowable time step at each cell. This is called *local time stepping.* Both of these techniques are described below.

4.2.1 Time Marching Scheme

Assuming the grid within the domain remains fixed, then the Euler operator may be written in the form

$$\frac{d}{dt}\{AW\} + P\{W\} = 0, \tag{4.18}$$

where $P\{W\}$ is the combined spatial and dissipation operator. Time marching of the result is obtained by using a multistage Runge-Kutta type technique. The first stage is an Euler predictor half step,

$$W^{n+*} = W^n - \frac{\aleph \Delta t}{2A}(P\{W^n\}). \tag{4.19a}$$

This stage is followed by a backward Euler corrector half step,

$$W^{n+**} = W^n - \frac{\aleph \Delta t}{2A}(P\{W^{n+*}\}). \tag{4.19b}$$

The third stage is a full step midpoint rule predictor,

$$W^{n+***} = W^n - \frac{\aleph \Delta t}{A}(P\{W^{n+**}\}). \tag{4.19c}$$

Finally, the next time step is obtained from a full step Simpson's rule corrector,

$$W^{n+1} = W^n - \frac{\aleph \Delta t}{6A}(P\{W^n\} + 2P\{W^{n+*}\} + 2P\{W^{n+**}\} + P\{W^{n+***}\}). \quad (4.19d)$$

Here, $\aleph$ is the CFL number, which for stability reasons must be less than $2\sqrt{2}$. The time step for each cell is given by,

$$\Delta t = \left[\frac{|u| + a}{\Delta \tilde{x}} + \frac{|v| + a}{\Delta \tilde{y}}\right]^{-1} \quad (4.20)$$

where a is the local sound speed and $\Delta\tilde{x}$ and $\Delta\tilde{y}$ are the minimum cell dimensions.

4.2.2 Time Accurate Solutions

The mulitstage technique described above can be used to obtain fourth order accurate time integration. This is done by setting the CFL number to unity, ($\aleph = 1$), and using a time step that is less than the most restrictive cell step,

$$\Delta t \leq \text{MIN}\left\{\left[\frac{|u| + a}{\Delta \tilde{x}} + \frac{|v| + a}{\Delta \tilde{y}}\right]_{i,j}^{-1}\right\}. \quad (4.21)$$

Since the dissipation is a spurious factor it is not necessary to recompute it at each stage of the Runge–Kutta scheme. This allows for less computational effort while still maintaining time accuracy.

The solution is marched forward in time from some starting solution, which should be physically accurate. For flows which are perturbations to a steady state the starting solution can be the steady state solution. For other flows, however, the starting solution might be the stagnation condition. The latter case is unfortunate because it leads to lengthy and expensive computational runs.

4.2.3 Asymptotic Steady State

For flows where it is suspected that there is a steady state solution, it is possible to accelerate the scheme. For this case the largest possible CFL number is chosen and each cell is advanced at its maximum time step. As in the previous case, the computational effort can be decreased by freezing the dissipation to the first stage value. For the majority of cases to be presented here, the algorithm was run in this fashion.

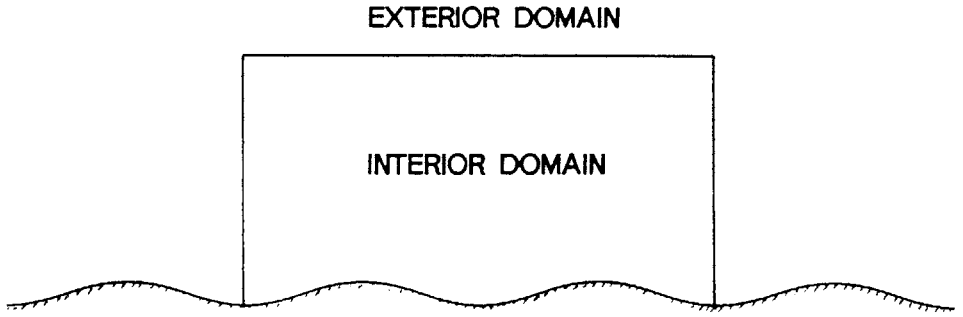

Figure 4.1: Solution Domain for a Wavy Wall

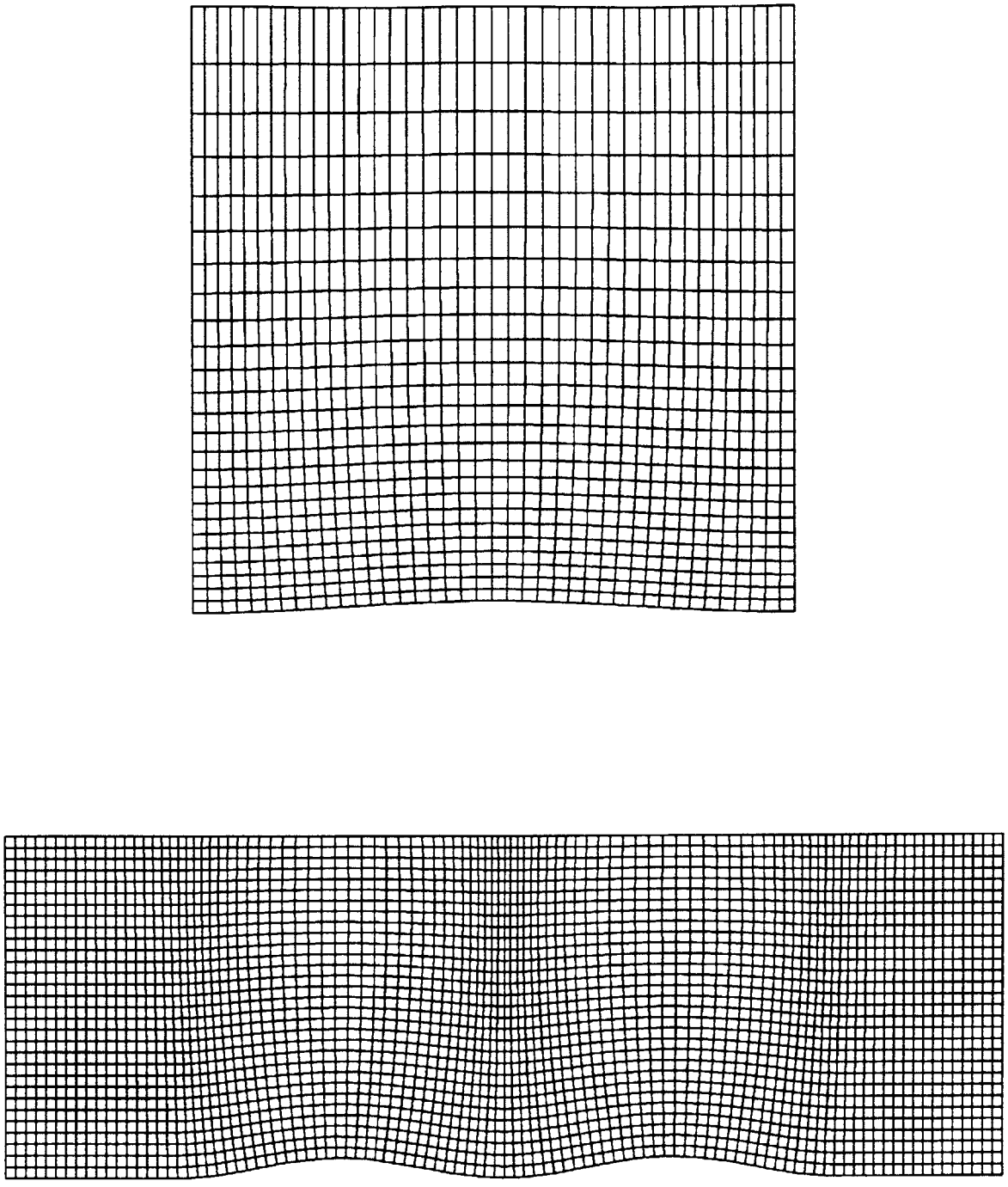

Figure 4.2: Sample Grids Using Equation (4.7)

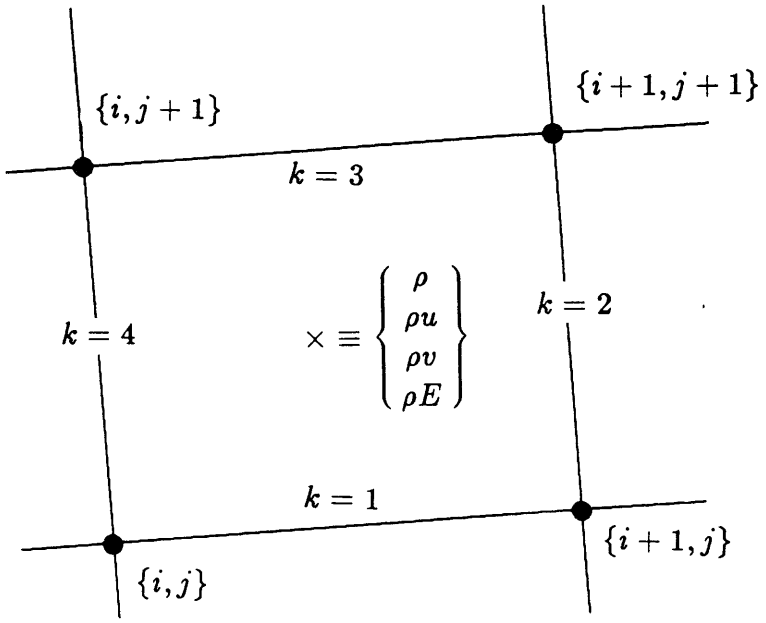

Figure 4.3: Representative Cell

Chapter 5

NUMERICAL BOUNDARY CONDITIONS

To obtain a unique solution to the wavy wall problem using the numerical algorithm described previously it is necessary to add numerical boundary conditions. These conditions are applied at some arbitrary grid boundary, see Figure 5.1. Unfortunately, the analytic boundary conditions are not always defined at the same location. Therefore, great care must be exercised when implementing certain boundary conditions, particularly inflow and outflow conditions. Thankfully, solid wall and periodic boundary conditions are not as difficult. These conditions will be described first. The general formulation for one dimensional characteristic boundaries will then be reviewed. This is followed by a description of the linearized conditions and the Riemann invariant formulation. Finally, application of the boundary conditions will be discussed.

5.1 Solid Wall Boundary Conditions

For those cells which have faces on the wavy wall it will be necessary to apply the solid wall boundary conditions given by equations (3.5) and (3.6). As shown previously, this implies that the pressure on the face is known. The pressure on these faces is

obtained from the normal momentum equation

$$\left(\frac{\partial P}{\partial \eta}\right)_{body} = \left(\frac{\rho q^2}{R}\right)_{body} \tag{5.1}$$

where R is the local wall curvature. Here the velocity at the wall, Figure 5.2, can either be obtained by taking the cell center value or it may be extrapolated from the interior using a second order Taylor expansion,

$$(\rho q^2)_{body} = \frac{(\rho q^2)_1 \Delta\eta_2 - (\rho q^2)_2 \Delta\eta_1}{\Delta\eta_2 - \Delta\eta_1}. \tag{5.2}$$

For the cases reported here the choice made little difference to the final solution. In general, however, the latter choice is superior and is used for the results presented.

The radius of curavture is determined by noting that for any surface described by $y = B(x)$, the curvature, $\Theta = \frac{1}{R}$, is given by

$$\Theta = \frac{B''(x)}{(1 + B'(x)^2)^{\frac{3}{2}}} \quad . \tag{5.3}$$

Substituting equation (4.1) into this result yields

$$\frac{1}{R} = \frac{-4\pi^2 \epsilon \sin(2\pi x)}{(1 + [2\pi\epsilon\cos(2\pi x)]^2)^{\frac{3}{2}}} \tag{5.4}$$

as the radius of curvature for the wavy wall.

Once a normal pressure gradient has been determined from equations (5.1) through (5.4), the pressure at the wall is found from the discretization

$$P_{body} = P_1 - \Delta\eta_1 \left(\frac{\partial P}{\partial \eta}\right)_{body}. \tag{5.5}$$

This technique gives a second order accurate computation for the pressure at a solid wall face.

5.2 Periodic or Repeating Conditions

It has been shown previously that the small perturbation solution to the wavy wall problem is periodic in space. While it seems unlikely that periodic flow will correctly represent the solutions for transonic and supersonic Euler wavy walls, it is possible that such solutions may exist for the subsonic case. Consequently, it will be informative to develop a periodic boundary condition for the algorithm.

Consider a grid, Figure 5.3, characterized by left and right boundaries which are displaced by exactly one wavelength, λ, of the wavy wall. If, as expected, the solution is periodic in the x direction, then it must be that

$$W(x+\lambda) = W(x) \tag{5.6}$$

Implementation of periodicity on the indicated grid implies that the left faces of the inflow cells must have the opposite flux values as the right faces of the outflow cells. Because a finite volume formulation with integration around the cell faces has been used, the periodic boundary condition is easily enforced. In particular, the averaging for the those faces, k, which are periodic, $k = \Im$, is obtained from

$$W_{\Im} = \frac{1}{2}\left(W_{1,j} + W_{imax,j}\right). \tag{5.7}$$

With this definition the flow that exits the right boundary will be convected back in the left boundary. It should be clear that this formulation has the distinct disadvantage of slow convergence. This is because the top boundary in now the only boundary through which spurious waves may escape the solution.

5.3 Characteristic Boundary Conditions

Application of the far field boundary conditions to an arbitrary grid boundary must be done with great care. It is necessary that any numerical boundary condition allow for both the correct solution near the wall and the nonreflection of spurious waves in the domain. It has been shown by Enquist and Majda[14] that this is easily accomplished by a one dimensional characteristic analysis. The analysis yields a set of invariant relationships for each of the characteristics. The number of boundary conditions specified at each numerical interface is then determined by the number of characteristics entering the numerical domain.

The linearized invariants to be outlined below have been derived in more detail by numerous authors[15][16][17]. Depending upon their implementation, the linearized equations have the disadvantage of being slightly reflective to spurious pressure waves. Improvement of this situation can be obtained by using the Riemann invariants instead. A derivation of this boundary condition will also be presented.

5.3.1 Linearized Invariants

The linearized characteristic equations are found by considering the one-dimensional Euler equations. Written in a natural coordinate system aligned with the boundary the primitive variable form of the Euler equations becomes,

$$\frac{\partial \tilde{W}}{\partial t} + \tilde{A}\frac{\partial \tilde{W}}{\partial x} = 0 \tag{5.8}$$

where,

$$\tilde{W} = \begin{Bmatrix} \rho \\ q_\eta \\ q_\xi \\ P \end{Bmatrix} \qquad \tilde{A} = \begin{Bmatrix} q_\eta & \rho & 0 & 0 \\ 0 & q_\eta & 0 & \frac{1}{\rho} \\ 0 & 0 & q_\eta & 0 \\ 0 & \rho a^2 & 0 & q_\eta \end{Bmatrix}. \tag{5.9}$$

Here, q_η and q_ξ are the normal and tangential velocities at the boundary. They are defined such that postive values correspond to inflow.

The characteristic form of the Euler equations is obtained by diagonalization of the primative variable form. Introducing a similarity matrix, $\tilde{S}$, equation (5.8) is written as

$$\tilde{S}^{-1}\frac{\partial \tilde{W}}{\partial t} + \tilde{S}^{-1}\tilde{A}\tilde{S}\tilde{S}^{-1}\frac{\partial \tilde{W}}{\partial x} = 0. \tag{5.10}$$

Equation (5.10) is next linearized by assuming that the similarity matrix is frozen and may be moved into and out of the derivatives. The resulting system has the form

$$\frac{\partial \tilde{C}}{\partial t} + \Lambda\frac{\partial \tilde{C}}{\partial x} = 0, \tag{5.11}$$

where Λ is a diagonal matrix composed of the $\tilde{A}$ matrix eigenvalues and $\tilde{C}$ is the vector of characteristic invariants for the Euler equations. If the eigenvalues of the matrix $\tilde{A}$ are given by, λ_n, then the diagonal matrix is found from the similarity martix using

$$\Lambda \equiv Diag(\lambda_1, \lambda_2, \lambda_3, \lambda_4) = \tilde{S}^{-1}\tilde{A}\tilde{S}. \tag{5.12}$$

The vector of boundary compatibility relations then follows from

$$\tilde{C} = \tilde{S}^{-1}\tilde{W}. \tag{5.13}$$

The eigenvalues of the matrix $\tilde{A}$ are given by the roots of the characteristic equation

$$|(\tilde{A} - \lambda I)| = 0, \tag{5.14}$$

where I is the identity matrix. Performing the indicated operations it can be shown that the eigenvalues are

$$\begin{aligned} \lambda_1 &= q_\eta \\ \lambda_2 &= q_\eta \\ \lambda_3 &= q_\eta + a \\ \lambda_4 &= q_\eta - a \end{aligned} \tag{5.15}$$

The similarity matrix is easily determined from this result by constructing the eigenvector for each eigenvalue. The inverse similarity matrix then follows, and can be used in equation (5.13) to determine the linearized compatibility equations,

$$\tilde{C} = \begin{Bmatrix} \rho - \frac{P}{\bar{a}^2} \\ q_\zeta \\ \frac{1}{\sqrt{2}}\left(q_\eta + \frac{P}{(\rho a)}\right) \\ \frac{1}{\sqrt{2}}\left(-q_\eta + \frac{P}{(\rho a)}\right) \end{Bmatrix} \tag{5.16}$$

Here, the barred quantities are values from the $\tilde{S}^{-1}$ matrix that are frozen quantities.

From equation (5.11) it is clear that $\tilde{C}$ is a vector of equations whose intrinsic derivatives along each characteristic are zero. These linearized compatibility relations are therefore invariant along the characteristics and are used to determine the linearized boundary conditions. Since derivation of the Riemann invariant form of the characteristic boundary conditions closely follows the presentation above, it will be presented before continuing with a discussion of how the characteristic boundary conditions are applied.

5.3.2 Riemann Invariants

The Riemann invariant form of the characteristic boundary conditions can be derived by considering a somewhat different form of the one dimensional Euler equations. Following the example of Moretti[18] and Zannetti[19], consider a locally isentropic formulation of the governing equations

$$\frac{\partial \ddot{W}}{\partial t} + \ddot{A}\frac{\partial \ddot{W}}{\partial x} = 0 \tag{5.17}$$

where,

$$\ddot{W} = \begin{Bmatrix} ln(P) \\ q_\eta \\ q_\zeta \\ s \end{Bmatrix} \qquad \ddot{A} = \begin{Bmatrix} q_\eta & \gamma & 0 & 0 \\ \frac{a^2}{\gamma} & q_\eta & 0 & 0 \\ 0 & 0 & q_\eta & 0 \\ 0 & 0 & 0 & q_\eta \end{Bmatrix}. \tag{5.18}$$

Here, s is the entropy of the flow, and the continuity equation has been written in terms of pressure by employing the isentropic flow relationship

$$\frac{dP}{P} - \gamma\frac{d\rho}{\rho} = 0. \tag{5.19}$$

The Riemann invariants are found, as before, by diagonalization of the governing equation,

$$\ddot{S}^{-1}\frac{\partial \ddot{W}}{\partial t} + \ddot{S}^{-1}\ddot{A}\ddot{S}\ddot{S}^{-1}\frac{\partial \ddot{W}}{\partial x} = 0. \tag{5.20}$$

Instead of linearizing the result, however, the actual similarity transformation is found.

Observe from equations (5.14) and (5.18) that the Riemann form has the same eigenvalues as the linearized form. If equation (5.20) is rewritten as

$$\ddot{S}^{-1}\frac{\partial \ddot{W}}{\partial t} + \ddot{\Lambda}\ddot{S}^{-1}\frac{\partial \ddot{W}}{\partial x} = 0, \tag{5.21}$$

where for convienence $\ddot{\Lambda}$ is defined as[20],

$$\ddot{\Lambda} = \ddot{S}^{-1}\ddot{A}\ddot{S} \equiv Diag(\lambda_4, \lambda_3, \lambda_2, \lambda_1) \tag{5.22}$$

then the similarity matrix takes the simple form

$$\ddot{S} = \begin{Bmatrix} \frac{-\gamma}{a\sqrt{2}} & \frac{1}{\sqrt{2}} & 0 & 0 \\ \frac{1}{\sqrt{2}} & \frac{a}{\gamma\sqrt{2}} & 0 & 0 \\ 0 & 0 & 1 & 0 \\ 0 & 0 & 0 & 1 \end{Bmatrix}. \tag{5.23}$$

Finally the diagonalized system is obtained by taking the matrix inverse,

$$\ddot{S}^{-1} = \begin{Bmatrix} \frac{-a}{\gamma\sqrt{2}} & \frac{1}{\sqrt{2}} & 0 & 0 \\ \frac{1}{\sqrt{2}} & \frac{\gamma}{a\sqrt{2}} & 0 & 0 \\ 0 & 0 & 1 & 0 \\ 0 & 0 & 0 & 1 \end{Bmatrix} \tag{5.24}$$

and substituting it into equation (5.21), yielding

$$\frac{1}{\sqrt{2}}\left\{\frac{\partial q_\eta}{\partial t} + \lambda_4\frac{\partial q_\eta}{\partial x} - \frac{a}{\gamma}\frac{\partial ln(P)}{\partial t} - \lambda_4\frac{a}{\gamma}\frac{\partial ln(P)}{\partial x}\right\} = 0 \tag{5.25a}$$

$$\frac{1}{\sqrt{2}}\left\{\frac{\gamma}{a}\frac{\partial q_\eta}{\partial t} + \lambda_3\frac{\gamma}{a}\frac{\partial q_\eta}{\partial x} + \frac{\partial ln(P)}{\partial t} + \lambda_3\frac{\partial ln(P)}{\partial x}\right\} = 0 \tag{5.25b}$$

$$\frac{\partial q_\zeta}{\partial t} + \lambda_2\frac{\partial q_\zeta}{\partial x} = 0 \tag{5.25c}$$

$$\frac{\partial s}{\partial t} + \lambda_1\frac{\partial s}{\partial x} = 0 \quad . \tag{5.25d}$$

The compatibility relationships are determined from the preceeding system by introducing the intrinsic derivative along the characteristic,

$$\left.\frac{\tilde{D}}{\tilde{D}t}\right|_{\lambda} = \frac{\partial}{\partial t} + \lambda \frac{\partial}{\partial x}. \tag{5.26}$$

In addition, it will be useful to note that for isentropic flow of a perfect gas,

$$\frac{a}{\gamma}\frac{\tilde{D}ln(P)}{\tilde{D}t} = \frac{2}{\gamma - 1}\frac{\tilde{D}a}{\tilde{D}t}. \tag{5.27}$$

Multiplying the first of equations (5.25) by the $\sqrt{2}$, the second by $\frac{a\sqrt{2}}{\gamma}$, and finally introducing equations (5.26) and (5.27) yields,

$$\frac{\tilde{D}q_\eta}{\tilde{D}t} - \frac{2}{\gamma - 1}\frac{\tilde{D}a}{\tilde{D}t} = 0 \tag{5.28a}$$

$$\frac{\tilde{D}q_\eta}{\tilde{D}t} + \frac{2}{\gamma - 1}\frac{\tilde{D}a}{\tilde{D}t} = 0 \tag{5.28b}$$

$$\frac{\tilde{D}q_\zeta}{\tilde{D}t} = 0 \tag{5.28c}$$

$$\frac{\tilde{D}s}{\tilde{D}t} = 0 \tag{5.28d}$$

This system of equations may be written as

$$\frac{\tilde{D}\ddot{C}}{\tilde{D}t} = \frac{\tilde{D}}{\tilde{D}t}\begin{Bmatrix} q_\eta - \frac{2a}{\gamma-1} \\ q_\eta + \frac{2a}{\gamma-1} \\ q_\zeta \\ s \end{Bmatrix} = 0, \tag{5.29}$$

where $\ddot{C}$ is a vector containing the characteristic variables, which are invariant along the characteristics.

5.3.3 Applying Characteristic Conditions

The linearized and Riemann characteristic boundary conditions were previously derived. In each case, it was found that certain invariants or compatibility relationships were constant along the characateristic lines. The important results may be summarized in terms of those characteristics and their associated invariants,

$$\lambda = \begin{Bmatrix} q_\eta \\ q_\eta \\ q_\eta + a \\ q_\eta - a \end{Bmatrix} \qquad \tilde{C} = \begin{Bmatrix} \rho - \frac{P}{\bar{a}^2} \\ q_\zeta \\ \frac{1}{\sqrt{2}}\left(q_\eta + \frac{P}{(\bar{\rho}\bar{a})}\right) \\ \frac{1}{\sqrt{2}}\left(-q_\eta + \frac{P}{(\bar{\rho}\bar{a})}\right) \end{Bmatrix} \qquad \ddot{C} = \begin{Bmatrix} s \\ q_\zeta \\ q_\eta + \frac{2a}{\gamma-1} \\ q_\eta - \frac{2a}{\gamma-1} \end{Bmatrix} \tag{5.30}$$

Application of the boundary conditions using these results depends on whether the boundary has incoming or outgoing characteristics. Figure 5.4 illustrates the form of the characteristics for a boundary where $q_\eta > 0$ implies inflow. From the figure, it is seen that at a supersonic inflow boundary all the characteristics *originate* outside the numerical domain. For a supersonic outflow boundary, the reverse is true, and all the characteristics *originate* from within the boundary. If the inflow boundary is subsonic, then three of the characteristics *originate* exterior to the domain. At a subsonic outflow boundary, only one characteristic *originates* outside the domain and three *originate* within the domain.

Application of the boundary condition is performed by enforcing the correct conditions along the appropriate invariants. This means that the values of the primitive variables are to be determined by attaching the invariant equations to their *originating* locus and freezing the values there. Thus, if $\tilde{C}_c$ or $\ddot{C}_c$ are the boundary values of the

invariants for implementing the boundary conditions and C_o is the originating locus of the applicable characteristic for each invariant equation, then the boundary values of the primitive variables are obtained by simultaneous solution of the system

$$\tilde{C}_c = C_o \quad \text{or} \quad \ddot{C}_c = C_o \quad . \tag{5.31}$$

For supersonic flow the solution of (5.31) is straightforward. For subsonic flow, however, certain problems arise when trying to solve the equation set. Consequently, many authors implement the latter case by taking additional liberties with equations (5.30). This is particularly true, as will be discussed shortly, at the outflow, where one of the invariants is often replaced to simplify the implementation.

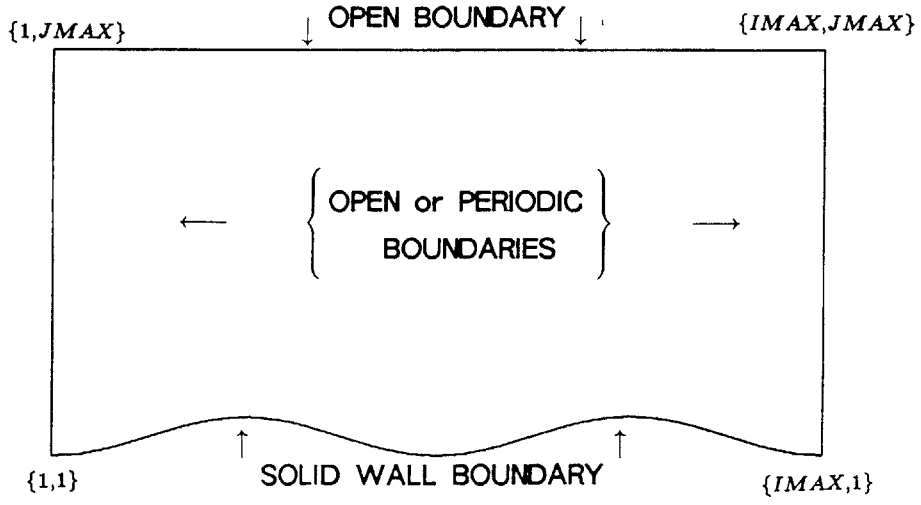

Figure 5.1: Grid Boundaries for the Numerical Scheme

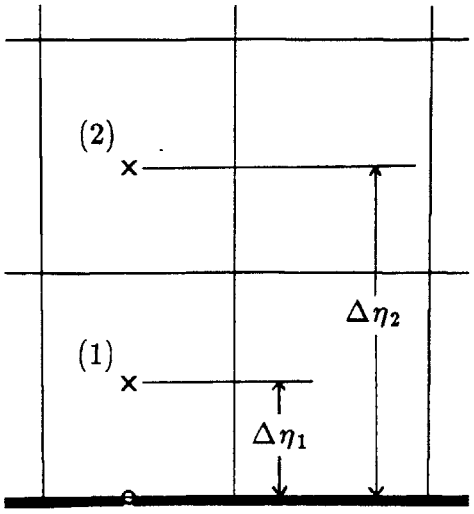

Figure 5.2: Pressure Extrapolation to the Wavy Wall

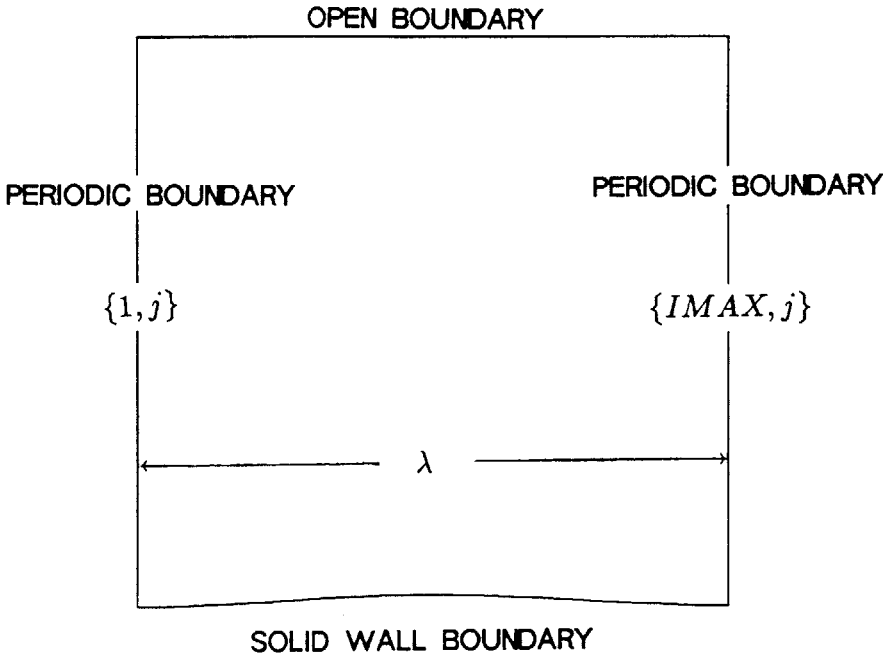

Figure 5.3: Boundaries for the Implementation of Periodicty

$$1 \Rightarrow q_\eta, \qquad 2 \Rightarrow q_\eta, \qquad 3 \Rightarrow q_\eta + a, \qquad 4 \Rightarrow q_\eta - a$$

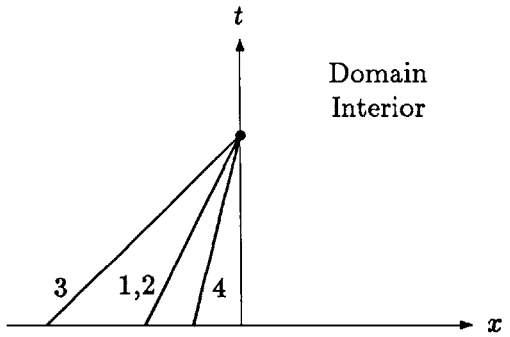

Supersonic Inflow — 4 b.c.

$q_n > 0, \quad |q_n| > c$

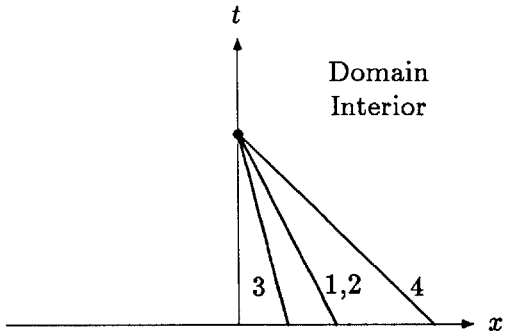

Supersonic Outflow — No b.c.

$q_n < 0, \quad |q_n| > c$

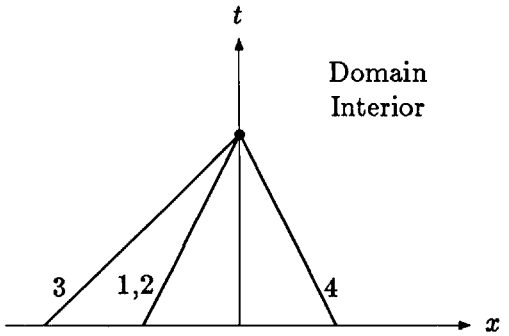

Subsonic Inflow — 3 b.c.

$q_n > 0, \quad |q_n| < c$

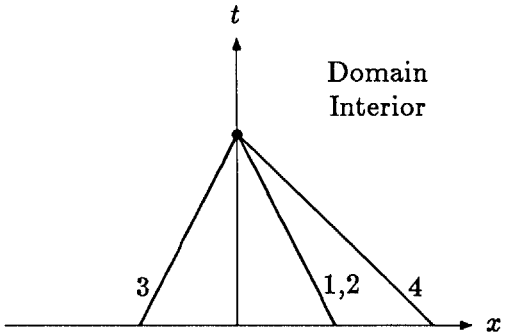

Subsonic Outflow — 1 b.c.

$q_n < 0, \quad |q_n| < c$

Figure 5.4: Characteristic Directions for 1–D Euler Equations

Chapter 6

IMPLEMENTING BOUNDARY CONDITIONS

The details of implementing the characteristic boundary conditions at those faces which lie along the *open* region of the grid are discussed. The formulation for supersonic cases is presented first. This is followed by a discussion of the simplifications often used for the subsonic case. The modified subsonic boundary conditions are then developed. This is followed by a discussion of the many options that can be used at the boundaries for the far field and frozen values. Finally, a discussion of how inflow and outflow boundaries are determined is presented.

6.1 Supersonic Boundaries

Consider a flow field where the velocity normal to the grid boundary is greater than the speed of sound, $|q_\eta| > a$. From the characteristics and invariants derived earlier

$$\lambda = \begin{Bmatrix} q_\eta \\ q_\eta \\ q_\eta + a \\ q_\eta - a \end{Bmatrix} \quad \tilde{C} = \begin{Bmatrix} \rho - \frac{P}{a^2} \\ q_\zeta \\ \frac{1}{\sqrt{2}}\left(q_\eta + \frac{P}{(\overline{\rho a})}\right) \\ \frac{1}{\sqrt{2}}\left(-q_\eta + \frac{P}{(\overline{\rho a})}\right) \end{Bmatrix} \quad \ddot{C} = \begin{Bmatrix} s \\ q_\zeta \\ q_\eta + \frac{2a}{\gamma - 1} \\ q_\eta - \frac{2a}{\gamma - 1} \end{Bmatrix} \tag{6.1}$$

it can be seen that if the boundary is an inflow boundary then all four characteristics *originate* at the far field. Consequently, all invariants should be fixed at their far field values. If the boundary is an outflow boundary then the four characteristics *originate* within the computational domain. For this case the invariants should be fixed at their interior values. An important point to be noted is that it is the normal velocity that must be supersonic. This is an important distinction for the supersonic wavy wall, where along the top boundary a subsonic boundary condition is used because the normal velocity is subsonic even though the total velocity is supersonic.

6.1.1 Supersonic Inflow and Outflow

For a supersonic inflow boundary all the characteristics enter the computational domain. Implementation of the boundary condition is performed by fixing the invariants at their far field values and then solving the set of simultaneous equations

$$\tilde{C}_c = \tilde{C}_{ff} \qquad \text{or} \qquad \ddot{C}_c = \ddot{C}_{ff}. \tag{6.2}$$

Here, C_c, are the boundary values and C_{ff} are the far field values. Fortunately, there is no need to perform this algebra. By setting the four primitive variables to their far field values the invariants for both forms are automatically satisfied.

Supersonic outflow is analogous to the inflow case. The only difference is that the invariants now originate within the domain. Consequently, the boundary condition is implemented by fixing the invariants at their interior values,

$$\tilde{C}_c = \tilde{C}_p \qquad \text{or} \qquad \ddot{C}_c = \ddot{C}_p. \tag{6.3}$$

Here the subscript, p, indicates values obtained by extrapolating the primitive variables from the previous Runge–Kutta stage to the appropriate boundary face.

6.2 Subsonic Boundaries

Consider now a boundary where the normal (positive for inflow) velocity is subsonic, $|q_\eta| < a$. The system of linearized equations obtained at the outflow boundary for this case contains some terms that are indeterminant. In addition, the Riemann equations contain a primitive variable not used by the numerical algorithm. To overcome these difficulties many authors[9][16][17][21] use the following modified set of equations

$$\lambda = \begin{Bmatrix} q_\eta \\ q_\eta \\ q_\eta + a \\ q_\eta - a \end{Bmatrix} \quad \tilde{C} = \begin{Bmatrix} \rho - \frac{P}{\bar{a}^2} \\ q_\zeta \\ \frac{1}{\sqrt{2}}\left(q_\eta + \frac{P}{(\bar{\rho}\bar{a})}\right) \quad \text{or} \quad P \\ \frac{1}{\sqrt{2}}\left(-q_\eta + \frac{P}{(\bar{\rho}\bar{a})}\right) \end{Bmatrix} \quad \ddot{C} = \begin{Bmatrix} \frac{P}{\rho^\gamma} \\ q_\zeta \\ q_\eta + \frac{2a}{\gamma - 1} \\ q_\eta - \frac{2a}{\gamma - 1} \end{Bmatrix} . \tag{6.4}$$

Here, the constant entropy condition in the Riemann equations has been replaced by an equivalent statement that $\frac{P}{\rho^\gamma}$ is a constant. In the linearized equations, an alternative third invariant has been introduced. The significance of the alternative choice, which will be used for the outflow boundary, will be explained shortly.

6.2.1 Linearized Inflow and Outflow

For an inflow boundary which has a subsonic normal velocity, three of the characteristics, (λ_1, λ_2, and λ_3), originate exterior to the computational domain. The re-

maining characteristic originates from within the domain. Correct determination of the primitive variables requires that those invariants originating from the exterior be fixed at their far field values. The remaining invariant is fixed by the interior values at the boundary face. The resulting set of simultaneous equations is

$$\begin{aligned} \rho_c - \tfrac{P_c}{\bar{a}^2} &= \rho_{ff} - \tfrac{P_{ff}}{\bar{a}^2} \\ q_{\xi c} &= q_{\xi ff} \\ q_{\eta c} + \tfrac{P_c}{\overline{\rho a}} &= q_{\eta ff} + \tfrac{P_{ff}}{\overline{\rho a}} \\ -q_{\eta c} + \tfrac{P_c}{\overline{\rho a}} &= -q_{\eta p} + \tfrac{P_p}{\overline{\rho a}} \end{aligned} \tag{6.5}$$

Here the subscript, c, indicates the boundary value to be determined , the subscript, ff, indicates far field values, and the subscript, p, indicates interior values. For the results reported, the interior values were obtained by first order extrapolation, to the cell face, of those values found at the previous stage of the Runge–Kutta time stepping. Discussion of possible far field values and frozen field values will be given shortly.

Simultaneous solution of equations (6.5) yields the primitive variables to be used by the numerical algorithm at the boundary faces

$$q_{\xi c} = q_{\xi ff} \tag{6.6a}$$

$$P_c = \frac{1}{2}\{P_{ff} + P_p + \overline{\rho a}(q_{\eta ff} - q_{\eta p})\} \tag{6.6b}$$

$$\rho_c = \rho_{ff} + \frac{1}{\bar{a}^2}(P_c - P_{ff}) \tag{6.6c}$$

$$q_{\eta c} = q_{\eta ff} - \frac{1}{\overline{\rho a}}(P_c - P_{ff}) \tag{6.6d}$$

Since this implementation of the boundary conditions is consistent with the invariants, the boundary should be nonreflective to plane pressure waves parallel to the boundary.

The subsonic outflow boundary is not as easy to implement as the inflow boundary. For this boundary there is one characteristic originating from the exterior region and three originating from within. Correct application of the boundary condition implies that the condition be implemented by solving the equation set

$$\begin{aligned} \rho_c - \tfrac{P_c}{\bar{a}^2} &= \rho_p - \tfrac{P_p}{\bar{a}^2} \\ q_{\zeta c} &= q_{\zeta p} \\ q_{\eta c} + \tfrac{P_c}{\bar{\rho}\bar{a}} &= q_{\eta ff} + \tfrac{P_{ff}}{\bar{\rho}\bar{a}} \\ -q_{\eta c} + \tfrac{P_c}{\bar{\rho}\bar{a}} &= -q_{\eta p} + \tfrac{P_p}{\bar{\rho}\bar{a}} \end{aligned} \tag{6.7}$$

for the primitive variables at the boundary faces. Unfortunately, because the far field value of q_η is not easily determined, this system of equations is difficult to implement. To overcome this problem, many authors replace this system with a modified set, obtained by discarding the third invariant

$$\begin{aligned} \rho_c - \tfrac{P_c}{\bar{a}^2} &= \rho_p - \tfrac{P_p}{\bar{a}^2} \\ q_{\zeta c} &= q_{\zeta p} \\ P_c &= P_{ff} \\ -q_{\eta c} + \tfrac{P_c}{\bar{\rho}\bar{a}} &= -q_{\eta p} + \tfrac{P_p}{\bar{\rho}\bar{a}} \end{aligned} \tag{6.8}$$

The usual arguement provided for making this modification is; *Since there is one incoming characteristic then one primitive variable can be specifed.* The modified set of equations is much easier to implement and yields the result

$$q_{\zeta c} = q_{\zeta p} \tag{6.9a}$$

$$P_c = P_{ff} \tag{6.9b}$$

$$\rho_c = \rho_p + \frac{1}{\bar{a}^2}(P_c - P_p) \tag{6.9c}$$

$$q_{\eta_c} = q_{\eta_p} + \frac{1}{\overline{\rho a}}(P_c - P_p) \tag{6.9d}$$

This boundary condition modification works quite well in practice, and it is not inconsistent with the steady state solution[22]. It is, however, physically inconsistent with the invariant approach. Consequently, there is no guarantee that this implementation is nonreflecting. In fact, the method at least partially reflects some of the spurious plane pressure waves. Because the reflected wave must exit some other boundary, the convergence rate of steady state runs using this technique will be adversely impacted. In addition, it is clearly not the best choice of a boundary condition for a time accurate computations.

6.2.2 Riemann Inflow and Outflow

Implementation of the boundary conditions using the Riemann invariants formally follows the same procedure decribed for the linearized invariants. At a subsonic inflow boundary, the primitive variables are obtained by simultaneous solution of the equation set

$$\begin{aligned} \left(\frac{P}{\rho^\gamma}\right)_c &= \left(\frac{P}{\rho^\gamma}\right)_{ff} \\ q_{\zeta_c} &= q_{\zeta_{ff}} \\ q_{\eta_c} + \tfrac{2a_c}{\gamma-1} &= q_{\eta_{ff}} + \tfrac{2a_{ff}}{\gamma-1} \\ q_{\eta_c} - \tfrac{2a_c}{\gamma-1} &= q_{\eta_p} - \tfrac{2a_p}{\gamma-1} \end{aligned} \tag{6.10}$$

given by attaching the appropriate invariants to the values for their originating locus. The solution of equation set (6.10) is made easier by introducing the definition of the

sound speed for an ideal gas

$$a^2 = \frac{\gamma P}{\rho}. \tag{6.11}$$

With the aid of the sound speed, the solution for the primitive variables then takes the form,

$$q_{\varsigma c} = q_{\varsigma ff} \tag{6.12a}$$

$$q_{\eta c} = \frac{1}{2}(q_{\eta ff} + q_{\eta p} + \frac{2}{\gamma - 1}[a_{ff} - a_p]) \tag{6.12b}$$

$$a_c = \frac{\gamma - 1}{4}(q_{\eta ff} - q_{\eta p} + \frac{2}{\gamma - 1}[a_{ff} + a_p]) \tag{6.12c}$$

$$\rho_c = \left\{ \frac{(a_c)^2 \rho_{ff}^{\gamma}}{\gamma P_{ff}} \right\}^{\frac{1}{\gamma - 1}} \tag{6.12d}$$

$$P_c = \frac{P_{ff} \rho_c^{\gamma}}{\rho_{ff}^{\gamma}} = \frac{(a_c)^2 \rho_c}{\gamma} \tag{6.12e}$$

The implementation for subsonic outflow is virtually identical. For this case the Riemann invariants take the form

$$\begin{aligned} \left(\tfrac{P}{\rho^{\gamma}}\right)_c &= \left(\tfrac{P}{\rho^{\gamma}}\right)_p \\ q_{\varsigma c} &= q_{\varsigma p} \\ q_{\eta c} + \tfrac{2a_c}{\gamma - 1} &= q_{\eta ff} + \tfrac{2a_{ff}}{\gamma - 1} \\ q_{\eta c} - \tfrac{2a_c}{\gamma - 1} &= q_{\eta p} - \tfrac{2a_p}{\gamma - 1} \end{aligned} \tag{6.13}$$

The primitive variables at the boundary faces are then determined from

$$q_{\varsigma c} = q_{\varsigma p} \tag{6.14a}$$

$$q_{\eta c} = \frac{1}{2}(q_{\eta ff} + q_{\eta p} + \frac{2}{\gamma - 1}[a_{ff} - a_p]) \tag{6.14b}$$

$$a_c = \frac{\gamma - 1}{4}(q_{\eta ff} - q_{\eta p} + \frac{2}{\gamma - 1}[a_{ff} + a_p]) \tag{6.14c}$$

$$\rho_c = \left\{ \frac{(a_c)^2 \rho_p^\gamma}{\gamma P_p} \right\}^{\frac{1}{\gamma-1}} \tag{6.14d}$$

$$P_c = \frac{P_p \rho_c^\gamma}{\rho_p^\gamma} = \frac{(a_c)^2 \rho_c}{\gamma} \tag{6.14e}$$

For both the inflow and the outflow results derived above, the equations for the primitive variables are consistent with the Riemann invariants. Consequently, correctly implemented boundary conditions using equations (6.12) or (6.14) will not reflect a plane pressure wave incident on the boundary. Assuming that all incident waves are parallel to the boundary, this implementation is much better for time accurate computations. However, this boundary condition will reflect an incident plane entropy wave[20] at the boundary if the interior solution is not isentropic. Fortunately, entropy reflections tend to settle down faster than pressure reflections.

6.2.3 The Far Field

In the foregoing analysis, the primitive variables for both the linearized and Riemann invariants are determined in terms of the far field values. What constitutes the far field values has not yet been addressed. In general, the far field may be described as that region exterior to the computational domain. Whether *exterior to the computational domain* means immediately exterior to it or infinitely far away form it is subject to interpretation. For the results presented below, two different interpretations of the far field values have been used.

Consider the case of flow past a wall consisting of one or more waves with a flat

region upstream and downstream, as shown in Figure 6.1. This configuration is very similar to that used by Ni[10], except that for this case the top boundary will be taken as being open, (*i.e.* it is an inflow – outflow boundary). For a case such as this, the far field will be interpreted as being the region infinitely far from the boundary. Conseqently, the nondimensionalized far field boundary conditions will be determined from

$$\begin{aligned} u_\infty &= 1 \\ v_\infty &= 0 \\ \rho_\infty &= 1 \\ P_\infty &= \frac{1}{\gamma M_\infty^2} \end{aligned} \tag{6.15}$$

It is important to note that the above far field implies that for the left and right boundaries,

$$\begin{aligned} q_{\eta ff} &= 1 \\ q_{\xi ff} &= 0 \end{aligned} \tag{6.16}$$

while for the top boundary it implies,

$$\begin{aligned} q_{\eta ff} &= 0 \\ q_{\xi ff} &= 1 \end{aligned} \tag{6.17}$$

The important point of this implementation occurs with the Riemann invariant boundary conditions at the outflow face. If the flow upstream of an outflow boundary contains a significant amount of total pressure loss then the boundary condition is wrong. This will result, as indicated before, in the reflection of an entropy wave from this bounadary. In this event, the time accuracy of a solution must be questioned.

An alternative far field definition is available if there is no flat region upstream and downstream of the waves. The idea is very similar to the compressible vortex correction used by some authors[15][16] to compute flow past an airfoil. For these cases the far

field conditions are computed from the potential wavy wall solution at the boundary. This boundary condition will be referred to as the near field condition. The velocities follow immediately from the boundary coordinates and equations (2.26) and (2.27) or (2.34) and (2.35). Densities and pressures are computed, assuming constant stagnation pressure and density, from the infinite far field values. The alternative approach can also be used along the top boundary when periodicity has been imposed on the left and right boundaries.

6.2.4 Selecting Frozen Values

For the boundary conditions implemented by using the equations which were linearized by freezing the similarity transformation, it is necessary to decide how the frozen field values will be obtained. There are numerous possibilities for obtaining these frozen field values. For example, they could be obtained from the infinite far field, or they could be taken as near field values computed from the potential solution. Other possibilities include using the values from the previous Runge-Kutta stage or those from the previous time step, $(n-1)$.

Since no choice is clearly superior, a numerical investigation was undertaken to see if any possibilty should be favored. For those cases tried, all the choices led to the same steady state result. Using the previous Runge–Kutta stage or the previous time step, resulted in slower convergence for some of the transonic cases. For this reason those two possibilities were eliminated.

For the linearized results reported herein, the frozen field values were taken to be the infinite far field values. The justification for this selection is that they needed to be computed only once, and therefore resulted in the least computational effort. In addition, this selection is consistent with the idea that the invariants are linearized about the freestream flow field.

6.3 Determining Inflow and Outflow

While it seems ludicrous to undertake a discussion of how to determine if a boundary is inflow or outflow, it turns out that this can have a large impact on the solution. There are three basic ways to determine which boundaries are inflow and which are outflow. The first method is to arrange the grid so that a given boundary is guaranteed to be of a certain type. The second method is to use some knowledge of what the solution is *supposed* to be to prescribe the boundary type. The final method is to allow the code to determine which boundaries are inflow and which are outflow.

An application of the first technique is the classic Ni[10] bump problem. In this problem the upper wall is a solid surface. This guarantees, for left to right flow, that the right face is an outflow boundary and the left face is an inflow boundary.

Application of the second method can be demonstrated by the wavy wall problem to be presented. For this problem only a portion of the top boundary is inflow. By knowing the potential solution, it is therefore possible to determine which portions are inflow and outflow. Observe that the full potential solution and not some guess is

required. This can be made clear by considering a guess like: the first half is outflow and the second half inflow. While this guess might work for the subsonic case it will not work for the supersonic case because the streamline crests at the top boundary may be out of phase with the solid wall wave crests.

Suppose that it is not possible to guarantee the boundary type and that no convenient guess for the solution exists. It will then be necessary to determine the boundary type from the flow velocites in the computational cells adjacent to the boundary. In fact, it would seem that this method is preferable, since the algorithm would then be self contained. However, as will be demonstrated below, this technique does not always work with the modified linearized invariants for very low Mach number flows. The cause appears to be related to a transient inconsistency between a wave reflecting off the outflow boundary and the method used to compute inflow and outflow along an adjacent boundary normal to the latter.

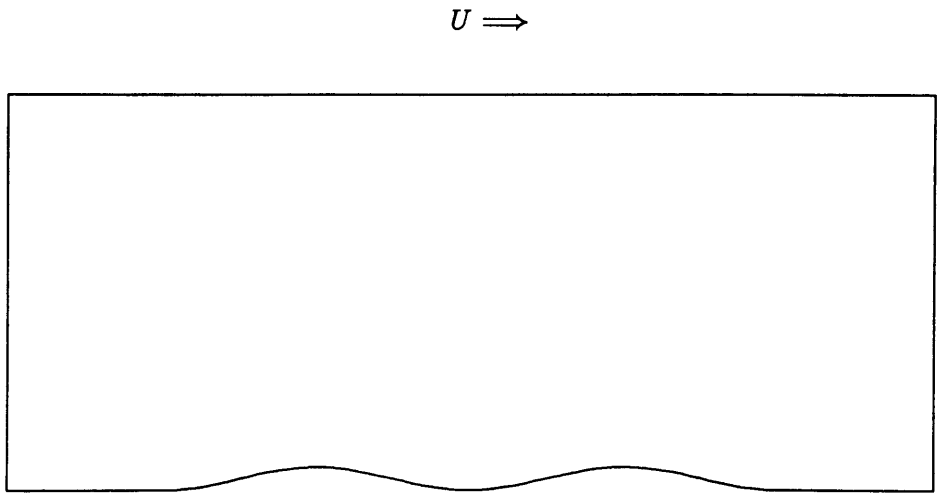

Figure 6.1: Flow Past a Ni Type Configuration.

Chapter 7

RESULTS

The results to be presented were selected to cover a range of possible flows over the wavy wall. For subsonic flows, the problem consists of a Mach 0.3 flow over a wave of amplitude, $\epsilon = 0.01$. The transonic solutions are obtained by using a Mach 0.775 flow past an $\epsilon = 0.025$ amplitude wave. The supersonic results are obtained for Mach 1.5 flow past waves of amplitude $\epsilon = 0.001$ and $\epsilon = 0.01$

The first solutions presented below are the results of the investigation into the differences between the linearized boundary condition with the modified outflow and the Riemann invariant boundary condition. These results confirm that in general the Riemann invariant conditions are a better boundary condition for the flows to be examined. Following the boundary condition investigation, the solutions to the multiple bump flows are presented. The multiple bump results demonstrate that for some flows the solution is not periodic in space over the entire domain. The multiple bump solutions are followed by the results obtained for subsonic flow by imposing the near field potential solution and by using periodic boundaries. These solutions are followed by the result obtained by using periodic boundaries to compute the transonic flow case. Finally, the results obtained while trying to compute the supersonic flow field are presented.

7.1 Invariant Boundary Condition Investigation

A comparison of the linearized invariant and Riemann invariant boundary conditions was performed to determine the relative merits of the two choices. The comparision examines the differences in convergence history and final solutions for a number of example computations. The comparisons are made using subsonic and transonic flows over a single wave with three free or open boundaries.

7.1.1 Convergence Comparison

Figure 7.1 shows the results of a comparison between the two boundary conditions obtained on a isolated transonic bump along a flat wall. The bump consists of a unit wavelength sine wave with an amplitude of $\epsilon = 0.025$. The maximum height of the bump relative to the flat wall is therefore, $\Delta y_{max} = 0.05$. The solution is obtained on the grid shown using a free stream Mach number of $M_\infty = 0.775$. As has been noted previously, because there is about a two percent total pressure loss in the solution there must be a reflected pressure wave in the linearized invariant result and a reflected entropy wave for the Riemann invariant result. The comparison shows that while the steady state solution is identical for both boundary conditions the convergence of the linearized case is much slower. This is consistent with previous comments about the reflectivity of the pressure waves for the linearized equations *vs* the reflectivity of the entropy waves for the Riemann equations. Finally, note that although the outflow far field characteristic is being set incorrectly the solution is identical to the result obtained using the pressure condition. Figure 7.2 demonstrates that a similar result can be expected for the subsonic

cases. In this figure the subsonic flow over a sine bump of amplitude $\epsilon = 0.01$ (total displacement of $\Delta y_{max} = 0.02$), and free stream Mach number $M_\infty = 0.3$ is shown. In addition, this flow has been computed by modifying the algorithm so that along the top boundary the first half is outflow and the second half is inflow. The reason for making this change, which was previously discouraged, will become clear in the next section.

7.1.2 Transient Phenomena

While examining the differences between the two boundary conditions, certain transient phenomena were observed along the upper boundary. The phenomena impacted the computations only for low speed subsonic flow employing the linearized invariants when the inflow – outflow condition was determined from the interior values. Figures 7.3 and 7.4 illustrate two of the transients that were observed.

In Figure 7.3 the convergence history is shown for the same case given in Figure 7.2 with the exception that inflow and outflow are now determined from the cell center values and not the guess. Observe that while the computed Mach number contours appear to be acceptable the solution will not converge to the desired convergence criteria. Attempts to change the damping and time stepping resulted in much the same situation, although the number of iterations is somewhat different. Examination of the detailed output for this run shows that some of the velocity vectors along the portion of the top boundary that should be outflow are oscillating. This results in the algorithm alternately treating those faces first as inflow and then outflow. If the inflow – outflow condition for the top boundary is presumed to be known, as was done in Figure 7.2, then the transient can

be eliminated.

Figure 7.4 shows the result of the computation for the same geometry as the previous case with an elogated upstream and downstream region. As in the previous computation the linearized boundary condition with the modified outflow is being used. Unlike the previous example, the Mach number contours for this computation are clearly unacceptable. Again the algorithm is having convergence problems along the top boundary. For this computation, in addition to the problem noted previously, the detailed output also shows that near the downstream boundary, where the flow should be inflow, the algorithm is employing the outflow boundary condition. For this solution, however, there is no oscillation and the faces in this region retain there outflow orientation. This results in the apparent expansion that is occuring at the upper right corner.

For these computations it is *conjectured* that the reflection of a spurious pressure wave off the downstream boundary moves upstream in the flow field causing a small perturbation of the v component of the velocity. For very low Mach numbers the perturbation is sometimes large enough to change the sign of the normal velocity component at the cells immediately adjacent to the boundary. If the algorithm employs cell center values to determine which faces are inflow and which are outflow, the perturbations can cause the algorithm to ascribe the wrong boundary condition to some of the cells along the top boundary. Depending on the size of the transient, the algorithm either oscillates or remains in the incorrect orientation. In either event, the algorithm does not recover the correct boundary condition after the wave has passed. This results in additional

perturbations and the algorithm quickly reaches a condition where it will converge no further. If a potential solution or a *valid* guess is used to determine which cells are inflow and which are outflow the algorithm as no convergence problems, and no transient is observed in the solution. As noted before, it was this guessing that resulted in the linearized solution obtained in Figure 7.2, which is otherwise identical to the solution in Figure 7.3. In addition, Figure 7.2 also demonstrates that the Riemann invariant boundary condition, with cell center determination of inflow – outflow, does not suffer from the transient problem.

7.1.3 Discussion of the Comparison

Based on the foregoing results it is concluded that in general the Riemann invariant boundary conditions are the better choice for the problem under consideration. While these boundary conditions do reflect entropy waves, the entropy of the solution settles down more quickly than the pressure. Consequently, the solution using the Reimann invariants converges faster. Since the convergence rate is an important factor for the periodic and multiple bump problems, this information is very useful. In addition, the Riemann conditions were not sensitive to transients at the boundary cells. The reason for this can be seen by comparing equations (6.12) and (6.14). From these equations it is clear that for both inflow and outflow, the normal velocity at the boundary face is determined by exactly the same relationship. This is not true for the linearized equations, and may in part contribute to the observed transients or at least be responsible for the algorithms inability to recover. The exact nature of these transients, however, is

not known and further research is required to determine the validity of the conjecture.

As a consequence of the preceding discussion, all further computations, with one exception, will be performed using the Riemann boundary conditions. The one exception is a supersonic example for which neither of the boundary conditions is valid. This case will be presented in the discussion of the supersonic wavy wall results.

7.2 Multiple Bump Flows

Since it was suspected that some transonic and supersonic flows might not be periodic in space, a series of multiple bump solutions was attempted. For these solutions an initial flat wall is followed by twelve or more sinusoidally varying waves. The objective of these computations, which are computer intensive, is to determine if the flows do become periodic in space and if so, over what region of the domain are the flows periodic. The results to be presented include computations for flows which are subsonic, transonic, and supersonic. All the computations are performed using the Riemann boundary conditions, with the far field values corresponding to a uniform free stream flow. In addition, all grids are of the same density per unit wavelength as the grids to be used for the imposed near field and periodic results to be presented later.

7.2.1 Subsonic Result

Figure 7.5 illustrates the result obtained for the $M_\infty = 0.3$ subsonic wavy wall. The computation is performed on a grid which has a density of $i \times j = 30 \times 20$ per

wavelength over 12 waves with an upstream and downstream flat wall that are each 1.5 wavelengths long. The computation required 25.25 hours of CPU time on VAX 11/785. The top half of this figure illustrates the Mach number contours and the wall Mach number for the entire solution. The bottom half of the figure is a view expanded about waves 5 to 8 from the central region of the solution. The computation demonstrates that for subsonic flow, the solution is periodic over a wide range of the computational domain. Observe that the flow is not periodic over the first or last two waves of this solution. This is not to be expected since for these waves the flow is responding to the influence of the adjacent flat wall region. In addition, the solution in the central region shows good comparison to the potential solution for the same case.

Based on this result, at least two other solutions for the subsonic case will be tried. Because the solution compares to the potential result, a solution will be attempted using a single wave with the potential near field applied at the boundaries. In addition, the figure illustrates the solution is essentialy periodic for those waves aft of the second crest. Based on this observation, a solution with periodic boundary conditions will be attempted. The computation will be run long enough to allow the flow to be convected through the domain at least three times.

7.2.2 Transonic Result

Figure 7.6 illustrates the results obatined for the transonic computation. This computation is performed on a grid which has a density of 30×20 per wavelength over a domain consisting of 30 waves. Again an initial and terminating flat wall of 1.5

wavelengths has been added to the domain. The computation is done at a free stream Mach number of $M_\infty = 0.775$ with a wave amplitude of $\epsilon = 0.025$, and required 53 hours of VAX 11/785 CPU time. In terms of the Chang and Kwon[3] transonic similarity parameter this represents a flow for $K = 6.027$. The solution shows that initially the flow over the waves is not periodic. The first wave has a weak shock which generates some small total pressure loss. The flow over the next wave crest then produces a second but even weaker shock which adds an additional but smaller increment of total pressure loss. Succeeding wave crests also have shocks which become successively weaker and consequently generate less and less additional pressure loss. This decaying of the shocks and incrementing of total pressure loss continues until about the 22^{nd} wave crest, after which the flow is barely transonic (there is a sonic point on each crest). Further aft of this wave crest, as illustrated by the expanded view of wave crests 22 through 25 in Figure 7.7, the flow appears to be periodic in space. Over the first twenty two waves the solution has acquired an aggragate total pressure loss of about 3.0 percent. Again, the influence of the downstream flat wall can be seen on the last two waves. Based on this result, the transonic flow will be attempted using the periodic boundary conditions. For this computation the flow will be required to reenter the domain at least twenty-two times.

7.2.3 Supersonic Result

Figure 7.8 shows the solution past 12 sinusoidally varying waves of amplitudes $\epsilon = 0.001$ and $\epsilon = 0.01$, for a supersonic free stream of $M_\infty = 1.5$. Note, that for

illustrative purposes only the first 8 waves are shown in each figure. The grid density for these computations is 30×30 per wavelength with no exponential stretching of the grid in the y direction. The choice of a uniform grid for this computation was dictated by the potential solution which indicates perturbations which do not decay in the y direction. In each case the computation required aproximately 30 hours of VAX 11/785 CPU time. In both cases, the computed solution is not periodic in the flow direction. For the larger amplitude waves there is a significantly stronger compression than the potential solution predicts. Consequently, the total pressure is decreasing in the flow direction, and this may be causing the nonperiodicity. For the smaller waves, however, there is practically no total pressure loss, yet the flow is not periodic.

The results obtained for this case are somewhat inconclusive. The nonperiodicity of the larger wave could be caused by the entropy generation, but this does not explain the remaining result. Because of this conflict, both cases will be tried using the imposed and periodic boundary conditons. However, as will be explained later, neither solution is valid, because in both cases there is an inconsistency between the local flow field near the boundary and the form of the boundary conditions applied there.

7.3 Subsonic Wavy Wall Results

The subsonic wavy wall problem has been solved by two additional methods which offer an improvement in the computational effort. In the first method the linearized potential solution is used as a boundary condition. This method results in the fastest

time to convergence but is limited to solutions that are nearly potential and of small amplitude. The second method is to impose periodic boundaries in the flow direction. This technique is slower than the first technique, but it allows for flows which contain larger perturbations and/or entropy generation.

7.3.1 Imposed Near Field Result

The effects of imposing the potential solution on the boundary of the computational domain was studied to determine the validity of using this procedure to reduce the computational time requirements. The results to be presented are obtained by computing the near field values of the potential solution at the boundary face and then using these values as the far field values for the Riemann invariants.

The solution for the subsonic flow is compared to the potential flow solution in Figure 7.9. In this computation the potential solution has been applied using the technique described above for the three free boundaries surrounding the 0.01 amplitude wave. The free stream Mach number has been set to $M_\infty = 0.3$. The figure shows the convergence history, grid, and Mach number contours obtained for this solution. From the figure it can be seen that the result is obtained with minimal computational effort, (15 minutes of CPU time on a VAX 11/750). The obtained solution is very close to that for the potential flow, and compares fairly well to the solution obtained using multiple bumps.

7.3.2 Periodic Boundary Condition Results

The solution for the subsonic wavy wall with periodicity imposed between the left

and right boundaries has been obtained using two different top boundary conditions. Figure 7.10 illustrates and compares the Mach number contours and convergence histories for solutions obtained by imposing the potential result along the boundary and by allowing that boundary to be a free stream boundary. In both cases the solutions have been iterated a sufficient number of times to allow the flow to be convected through the domain at least three times. To be sure that the solution obtained is directly related to a true time scale, all periodic runs were performed by running the algorithm in its time accurate mode. The solutions are obtained on a VAX 11/750 and each required approximately 1 hour of CPU time. These solutions compare quite favorably to all the previous results for this same case.

7.4 Transonic Wavy Wall Results

For transonic flow along a wavy wall the solution has been obtained by imposing periodicity in the flow direction while allowing the upper boundary to be a Riemann free stream far field boundary. For this case it was felt that imposition of the potential solution, either on all three boundaries or along the top boundary, would not be accurate. The solution is obtained for a transonic low past a sinsusoidally varying wall of amplitude, $\epsilon = 0.025$, with free stream Mach number of $M_\infty = 0.775$, is shown in Figures 7.11 and 7.12. Figure 7.11 illustrates the convergence history and compares the Mach number contours for this case with those obtained for the multiple bump solution. The comparison in Figure 7.11 illustrates that the solution to the periodic problem compares quite well to that for the multiple bump case. Figure 7.12 shows the

grid and the comparison of the stagnation pressure loss for this case and the multiple bump case. The plot of stagnation pressure loss indicates that the 3.0 percent loss is being convected through the domain. The plots also show that there is a small numerical error near the wall. This error accounts for the variation seen in Figure 7.6. While the computational effort was moderate, (2.2 hours of CPU time on a VAX 11/785), it is still far less than the 53 hour effort required for the multiple bump solution to which it corresponds.

There is a rather subtle point that should be made about both this computation and the subsonic computation. In both cases the computations were iterated a fixed total time that was determined from the results of the multiple bump solutions. While the convergence histories, for these cases and the supersonic ones to be presented shortly, appear to level out as the solutions approach the periodic region, this is not a generalizable statement. This is because the solutions, by the very nature of the boundary conditions, must contain both left and right running vertical waves. These waves are associated with background dissipation and account for the oscillations seen in the convergence history. A more lengthy computation would show that the peak levels of these oscillations are converging. The solutions obtained are therefore essentially periodic. For these reasons it is clear that when computing a more general flow which is periodic in the flow direction it is necessary to consider not only the convergence history but also the time invariance of the solution at each iteration. Keeping this in mind, however, the above results illustrate that a cell centered finite volume formulation can be used to compute such flows.

7.5 Supersonic Wavy Wall Results

The solutions for the supersonic, $M_\infty = 1.5$, flow past a wavy wall are presented next. Recall that in computing this flow with multiple bumps the result was not periodic. The reason for this, however, was not clear. Because of this a number of attempts at computing the field were made using both the imposed near field boundary conditions and the periodic boundary conditions.

7.5.1 Imposed Near Field Results

The first set of computations has been performed by imposing the near field potential solution on two of the boundaries. For these computations the boundary condition has been imposed on the left and top boundaries only. The top boundary is subsonic, in the normal direction, and like the subsonic case is treated by using the near field results as the far field values in the Riemann boundary conditions. The left boundary is a supersonic inflow, for this boundary all the primitive variables can and have been set to the potential values. Finally, the right boundary is the usual supersonic outflow boundary, where all the values are extrapolated from the interior of the domain. The objective in treating the right boundary in this manner is to determine if the computed solution will result in a flow field that is periodic.

Figure 7.13 illustrates the Mach number contours, grid, and convergence history obtained by the above technique for the 0.001 amplitude wall. It is seen that the result is very close to being periodic and compares well to the potential solution. It does not,

however, compare to the result obtained for the multiple bump solution.

While the result for the 0.001 amplitude wall is encouraging, there appears to be a limit to the extent over which the technique is applicable. This is seen in Figure 7.14 where the supersonic results for a wall amplitude of 0.01 are presented. The free stream Mach number is the same as that used for Figure 7.13. The upper half of this figure illustrates the Mach number contours obtained for this solution using both the Riemann invariants and the linearized invariant boundary conditions. The corresponding potential solution was given in Figure 2.3. Observe, that neither solution is periodic and that in addition both solutions are reflecting the expansion wave off the top boundary. In particular, the reflection is occuring only in that region of the boundary which is an outflow face. The predicted compression is much stronger than the potential solution indicates and a plot of the total pressure loss would confirm this.

The strong compression that occurs in the computation indicates that, unlike the potential solution, the Euler solution is nonlinear. This fact can be used to explain the reflection along the top boundary. Recall, that in computing the supersonic potential solution, the function, $G(x - \Lambda y)$, which corresponded to the upstream running characteristics was set to zero. This implies that the value of the upstream (or left) running supersonic characteristic is everywhere equal to a constant. The value of this supersonic characteristic is plotted in the lower half of Figure 7.14. The contours indicate that the fields possess as much as a 10 percent variation in this characteristic. A similar plot of the result for the 0.001 amplitude wave shows less than a 0.1 percent variation.

For the larger amplitude wave the error in the supersonic characteristics is actually being introduced by the potential solution, which itself has more implied variation in the supersonic characteristics than is probably acceptable for the underlying asssumptions in its derivation. The reflection occurs because of the inconsistency that arises when the wrong two dimensional supersonic characteristic is enforced by a boundary condition which assumes one dimensional linear flow. The reason that the reflection from the Riemann invariant boundary condition appears to be weaker is probably due to either one or both of the following reasons. First, the Riemann boundary condition reflects entropy waves, while the linearized boundary condition reflects pressure waves. Secondly, the Riemann condition sets the characteristic to the potential value which is only slightly incorrect. The linearized boundary condition introduces an additional error by only setting the pressure.

7.5.2 Periodic Results

While the above result explains why the larger amplitude result is not periodic it does not necessarily explain the multiple bump solution for the small amplitude wave. In fact the problem is exactly the same. This can be verified by attempting a periodic solution of the small amplitude wavy wall problem to see if the result obtained for the multiple bump case can be reproduced. For this case the computation has been done for two different implementations of the Reimann boundary conditions along the top surface.

In Figure 7.15 the result obtained by using the linearized potential solution as the

far field values in the Riemann invariants along the top boundary is shown. This figure shows the iteration history and Mach number contours obtained. For this computation the variation in the upstream running characteristic implied by the potential solution is negligible. Consequently, the supersonic characteristics are set to their correct values. Thus, the solution does not exhibit any reflections and compares almost exactly to the potential solution.

Figure 7.16 illustrates the computed result for the same flow with the infinite far field values used in the Riemann boundary condition along the top wall. For this case there is an inconsistency between the correct supersonic characteristics and those implied by the boundary conditions. In this case a reflection of exactly the same form observed in the multiple bump solution, which uses this boundary condition, is observed. It is concluded that use of either the pressure or Riemann invariant boundary condition is not valid if the flow in the edge region is nonlinear, unless the two dimensional supersonic characteristics are known and can be supplied.

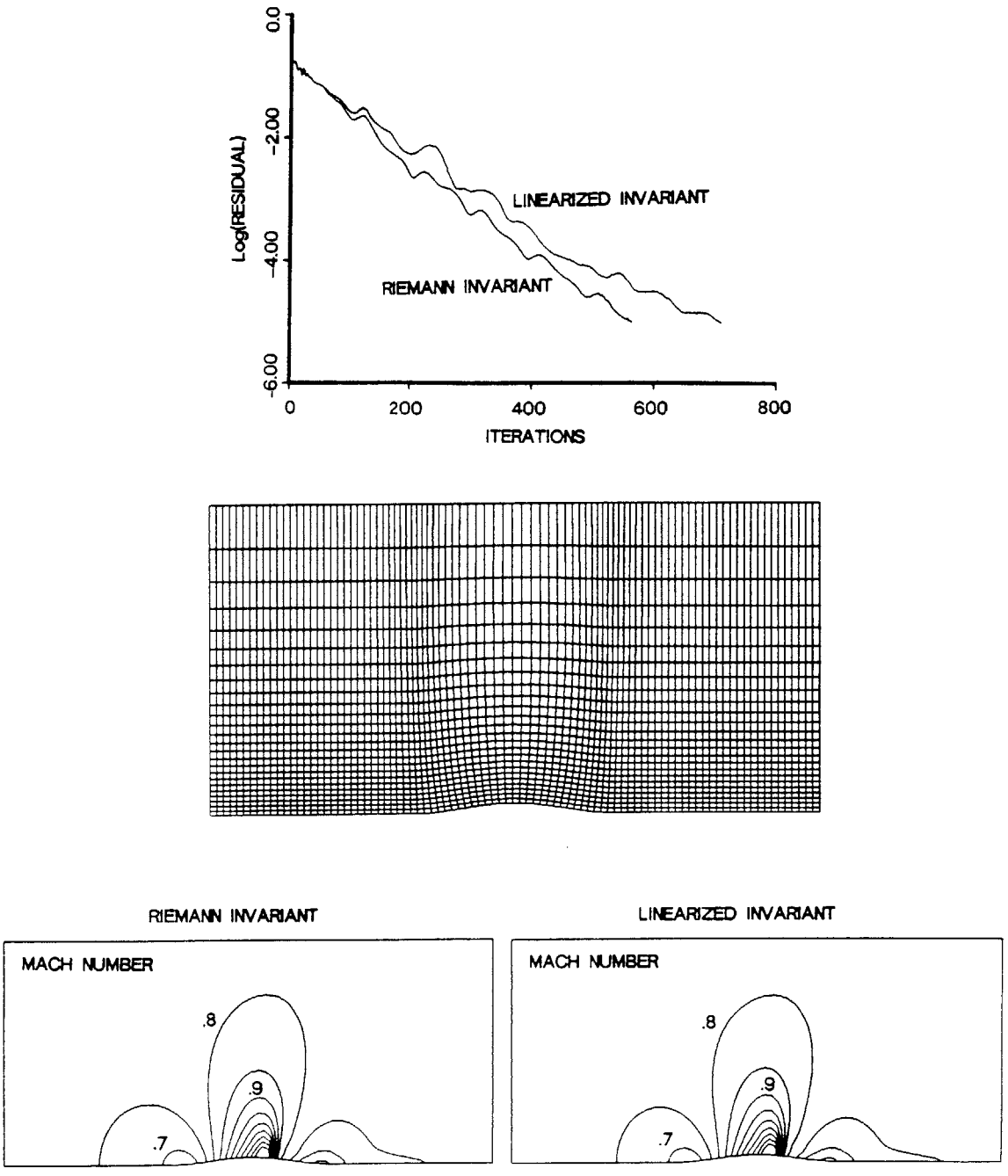

Figure 7.1: Transonic Flow Comparison, Free Boundaries.

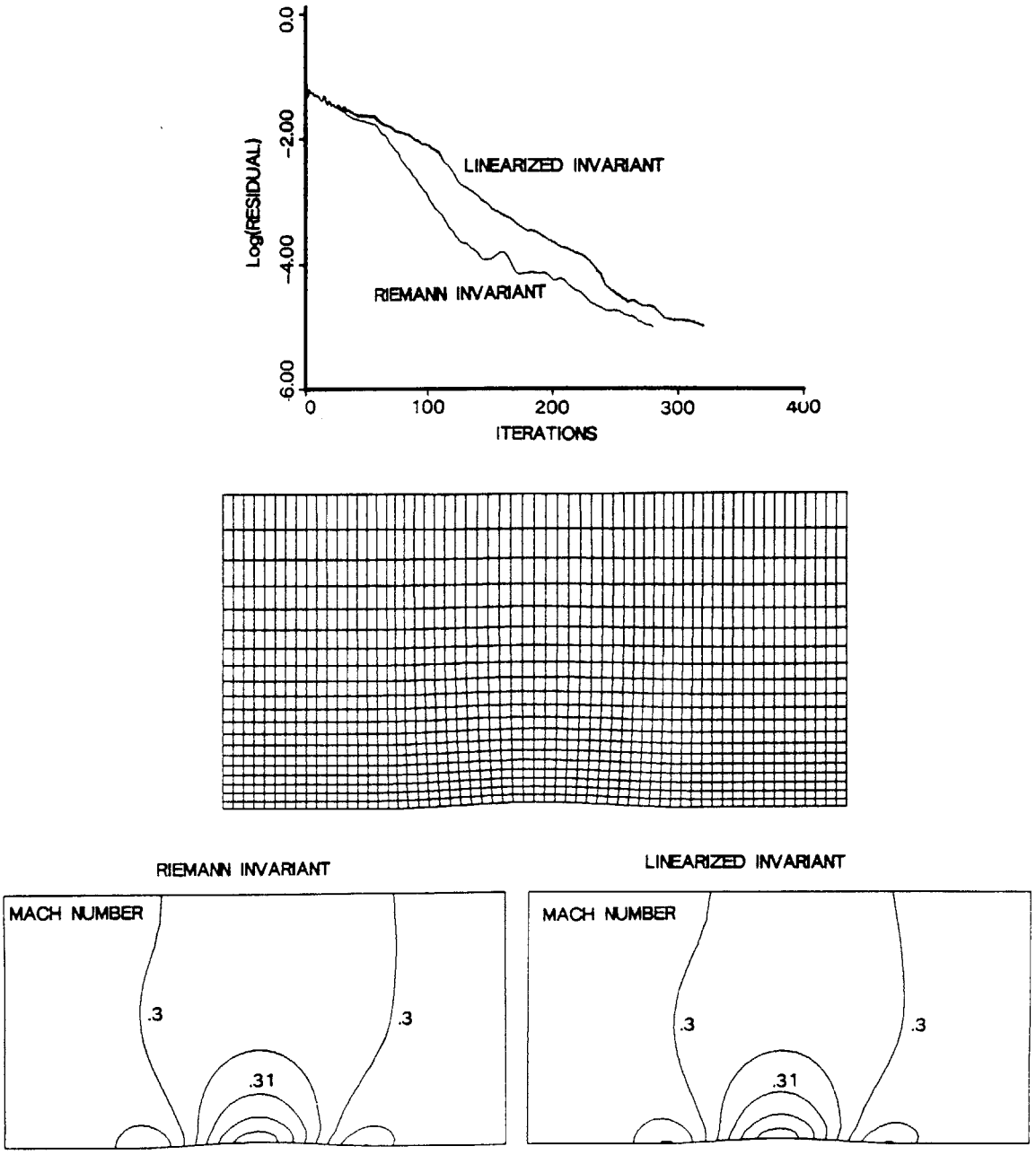

Figure 7.2: Subsonic Flow Comparison, Imposed Boundaries.

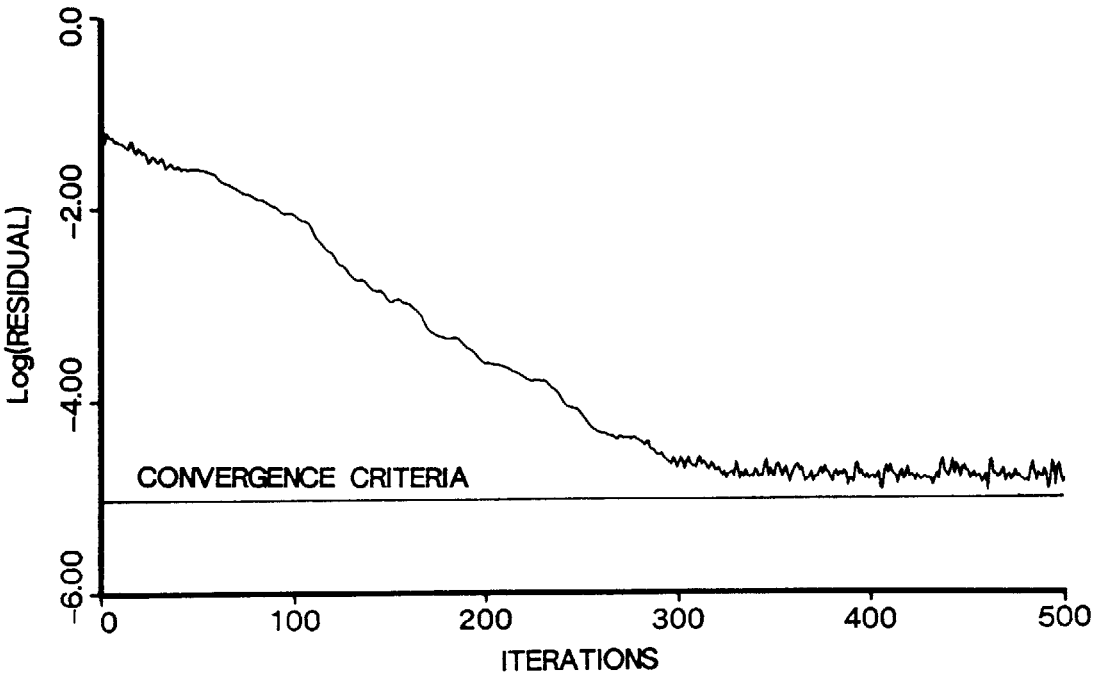

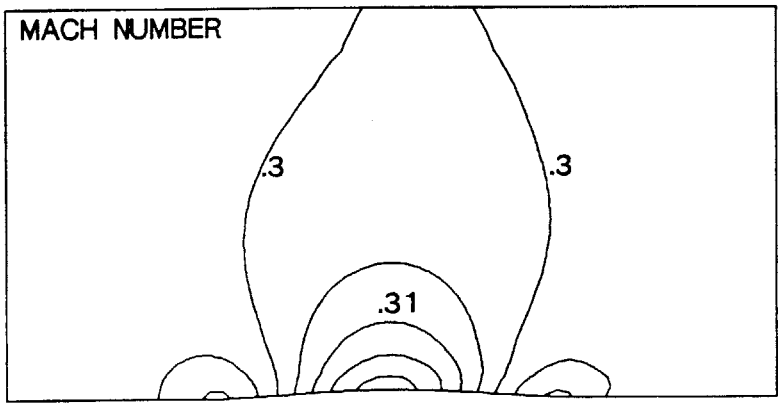

Figure 7.3: Subsonic Transient for Flow with Free Boundaries.

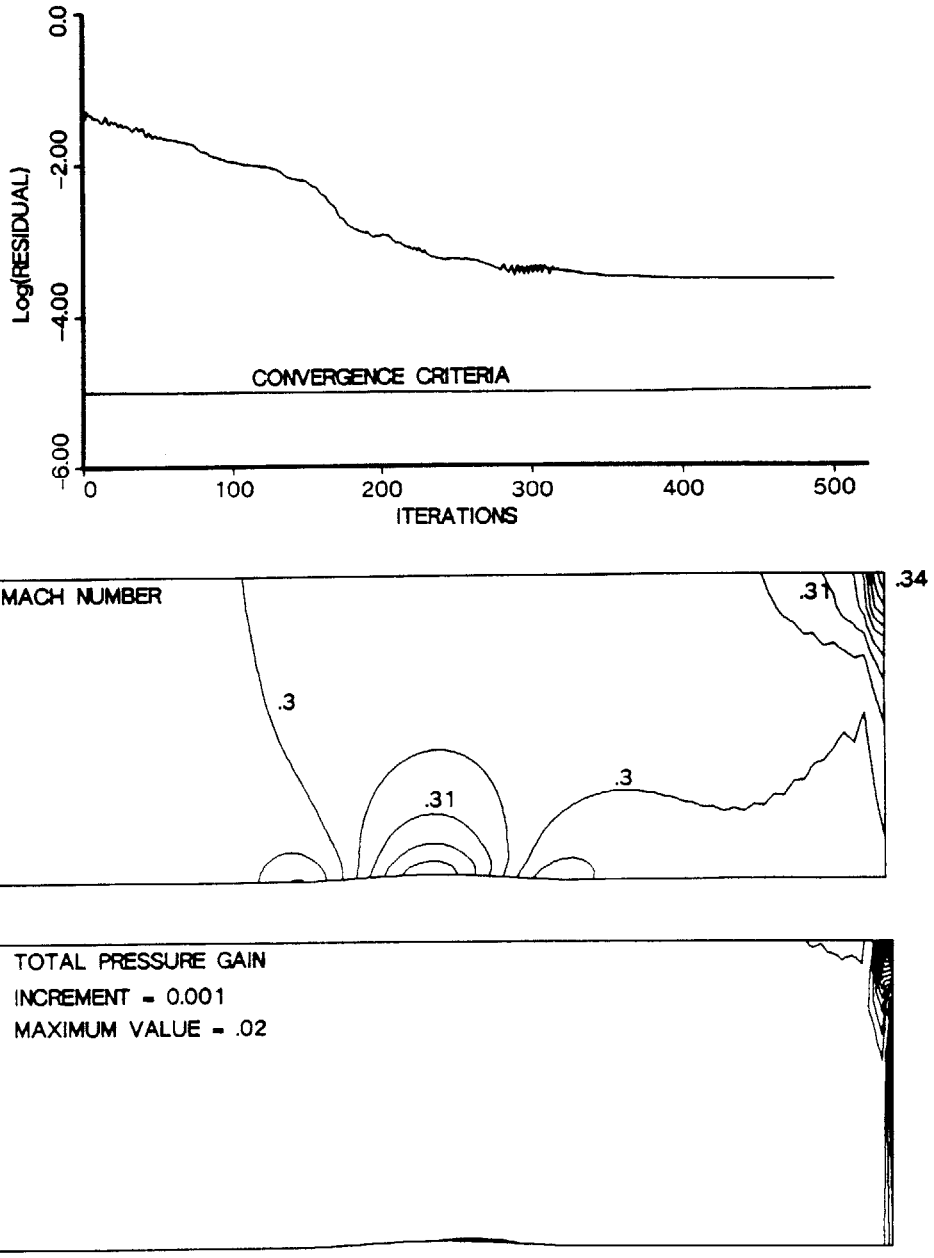

Figure 7.4: Subsonic Transient for Flow with Elongated Boundaries.

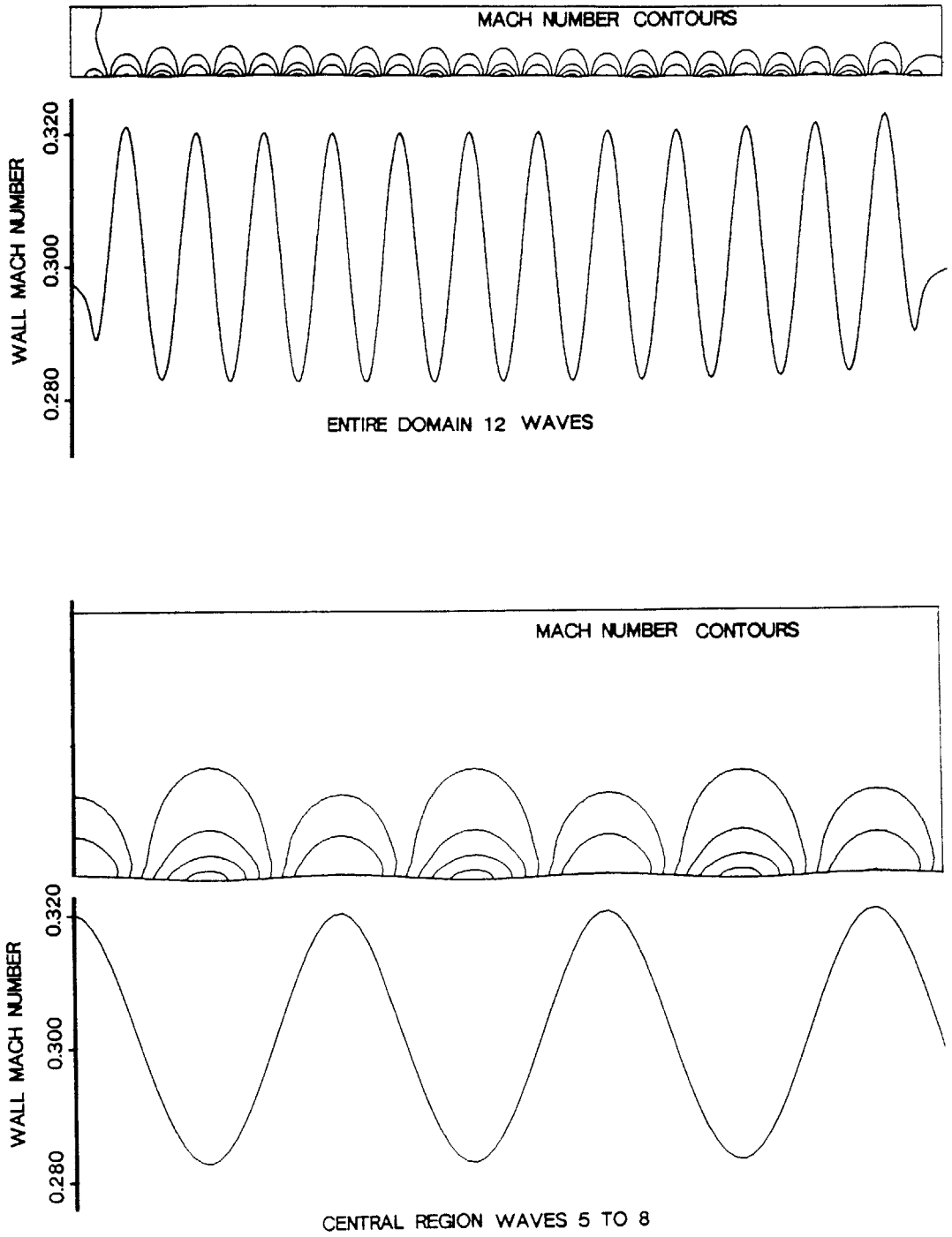

Figure 7.5: Subsonic Solution over 12 Waves, $M_\infty = 0.3$, $\epsilon = 0.01$.

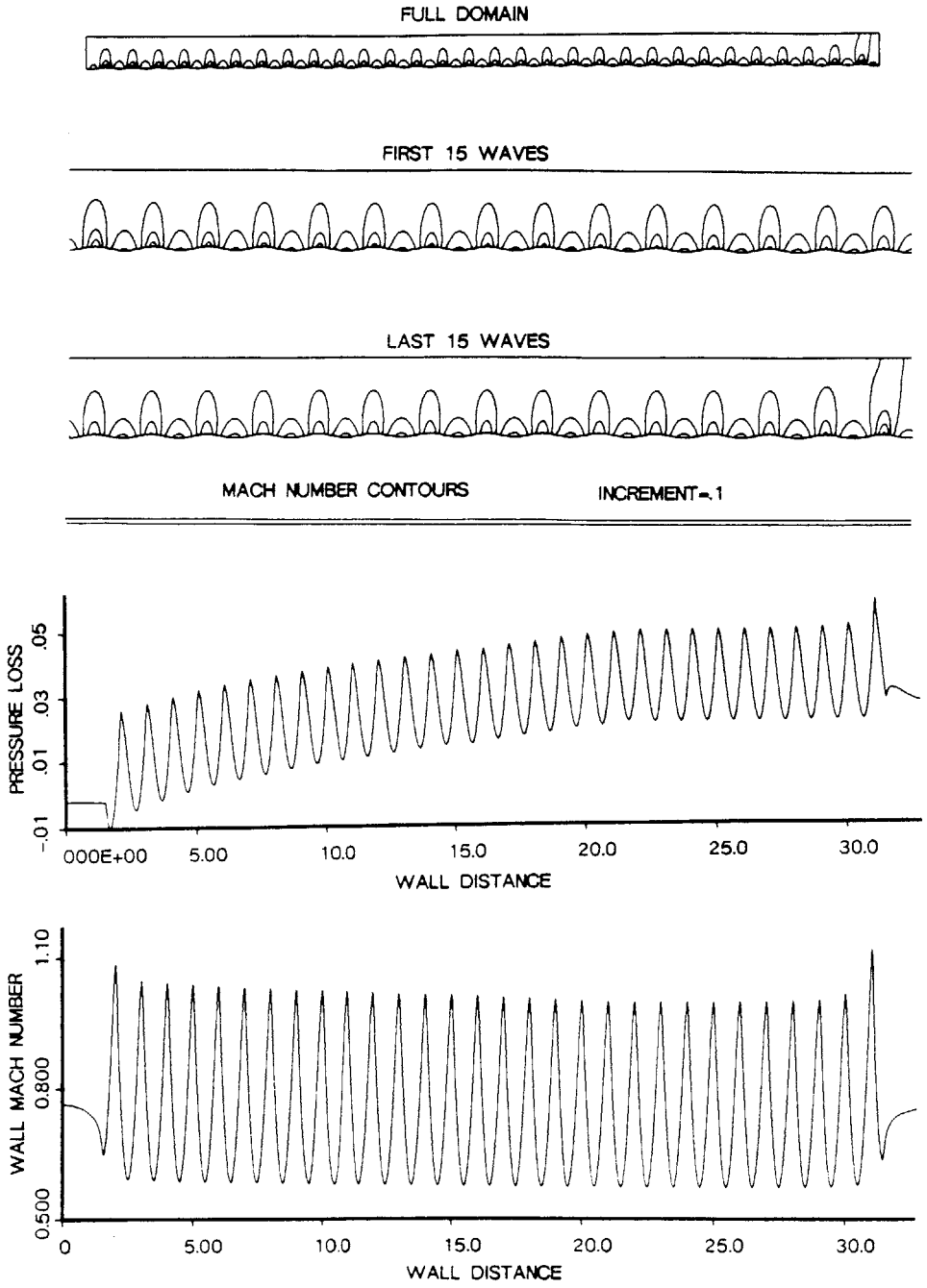

Figure 7.6: Transonic Solution over 30 Waves, $M_\infty = 0.775$, $\epsilon = 0.025$.

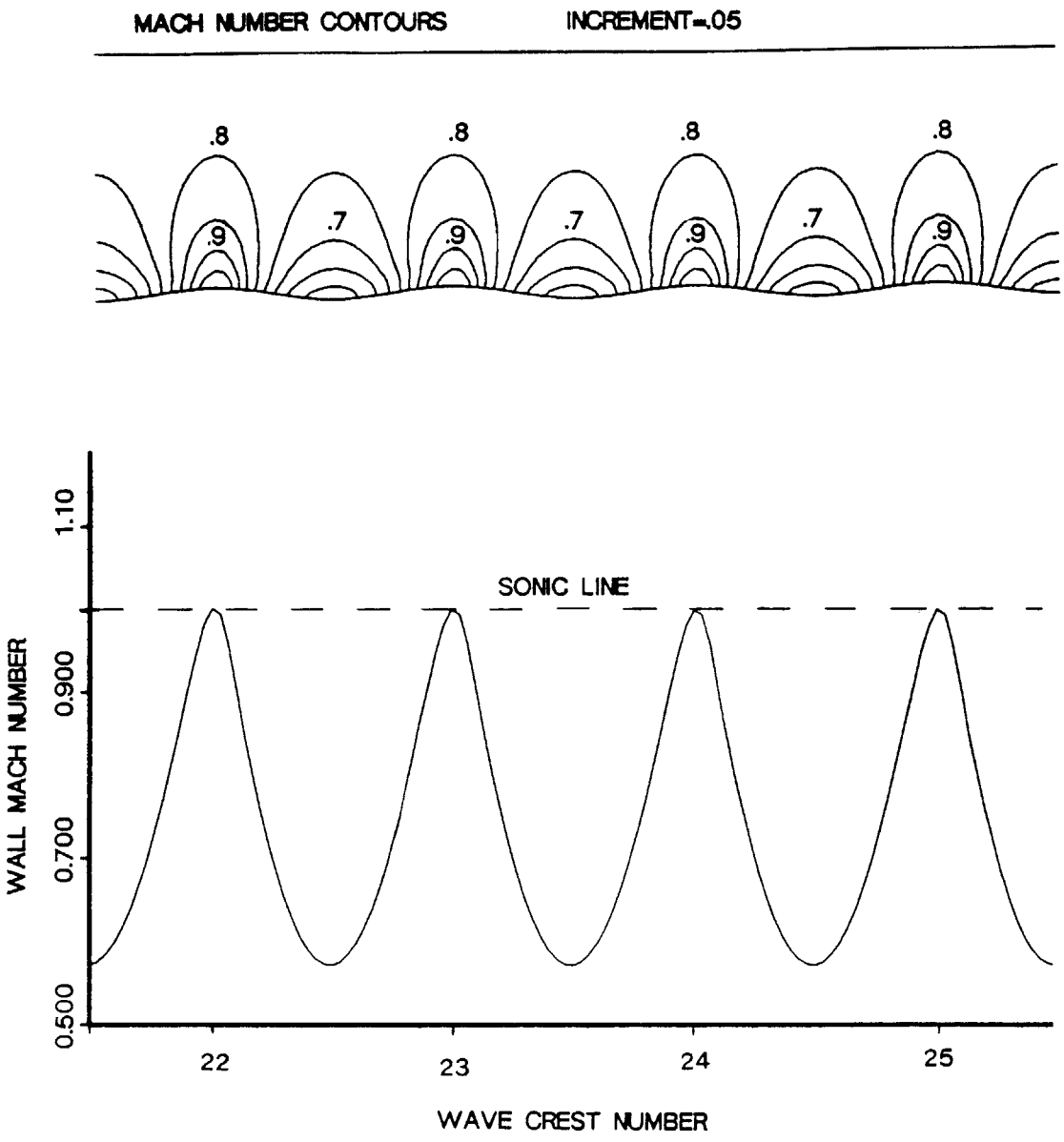

Figure 7.7: Exploded View of the Transonic Solution over Waves 22 to 25.

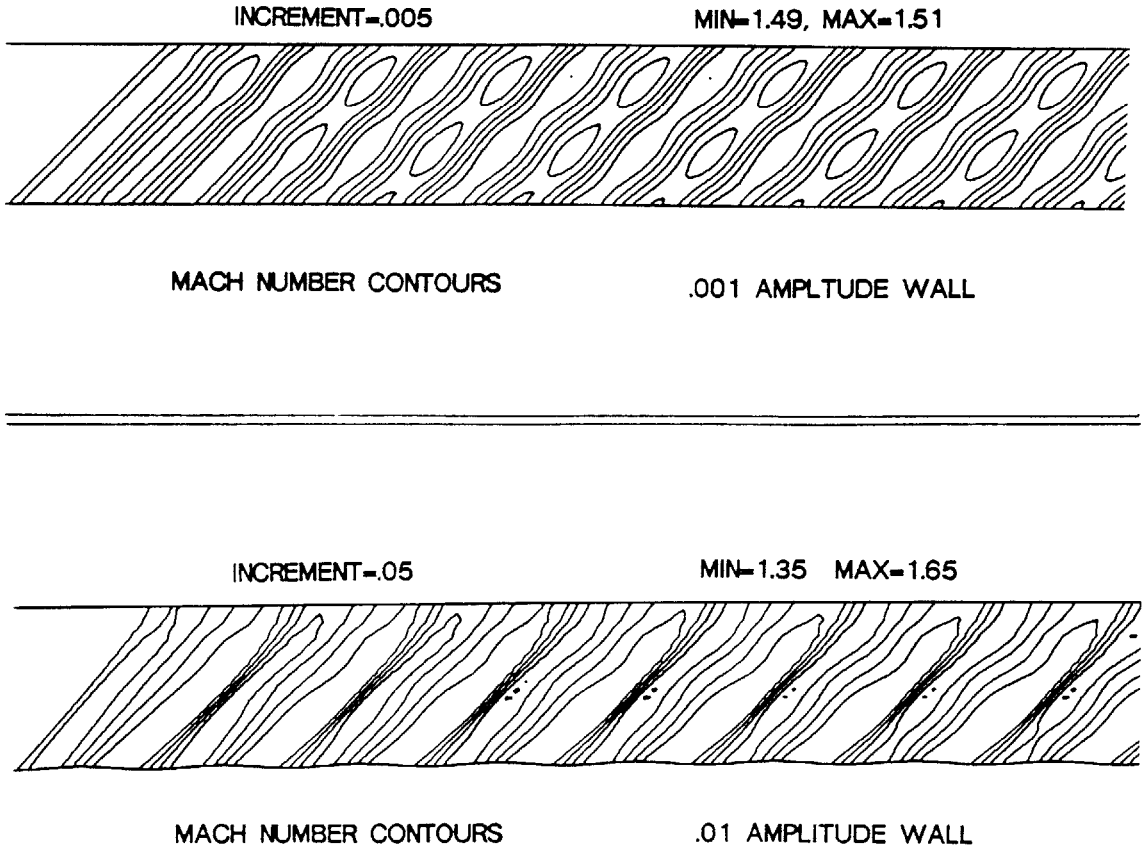

Figure 7.8: Supersonic Solution over the First 8 Waves of a 12 Wave Domain, $M_\infty = 1.5$.

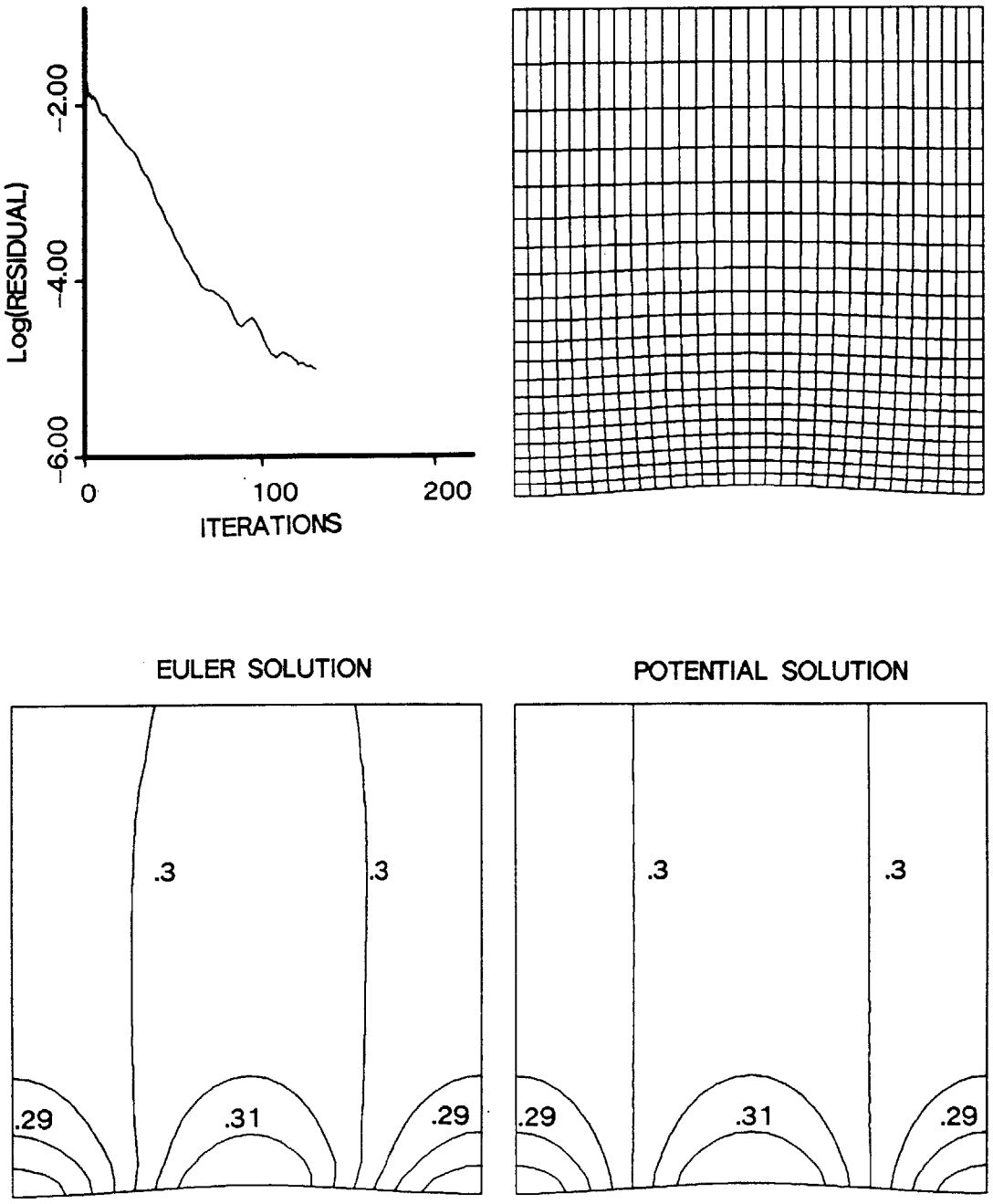

Figure 7.9: Subsonic Solution Using Imposed Boundaries, $M_\infty = 0.3$, $\epsilon = 0.01$.

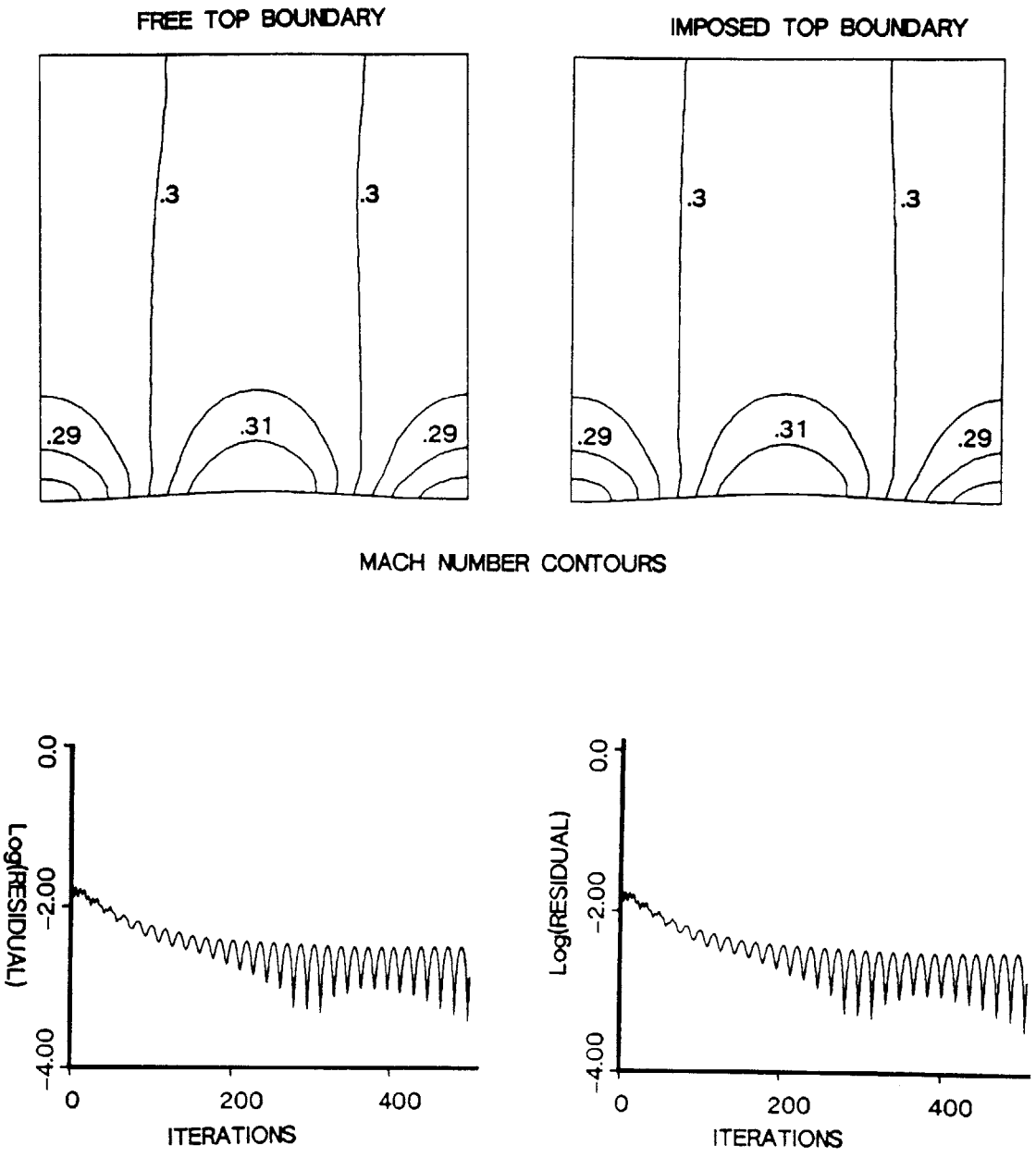

Figure 7.10: Subsonic Solution Using Periodic Boundaries, $M_\infty = 0.3$, $\epsilon = 0.01$.

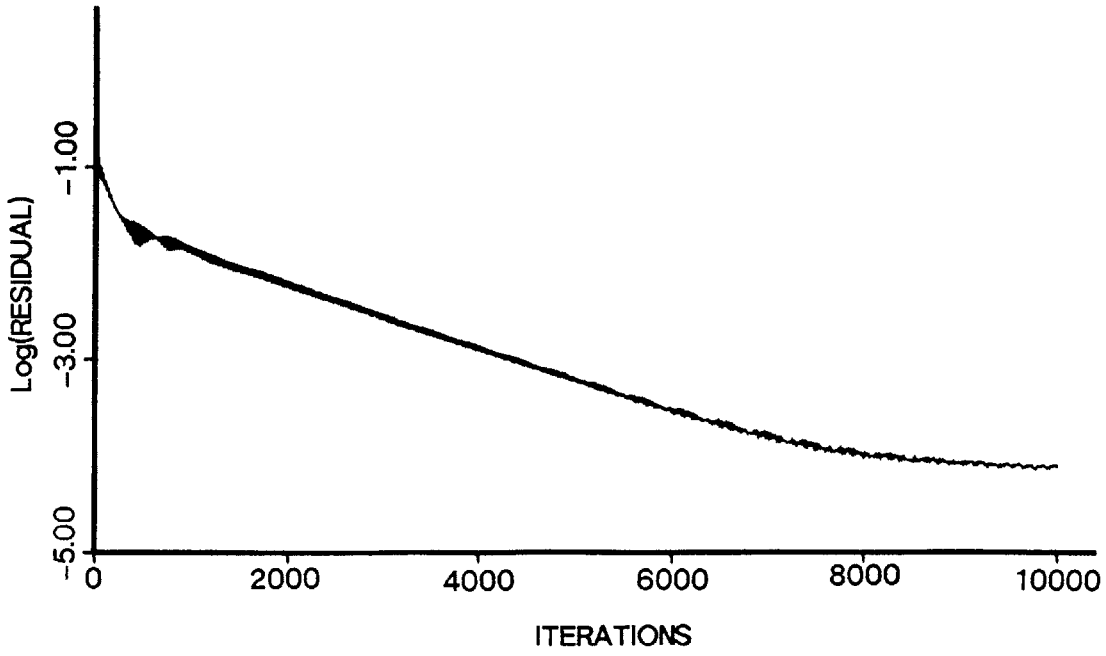

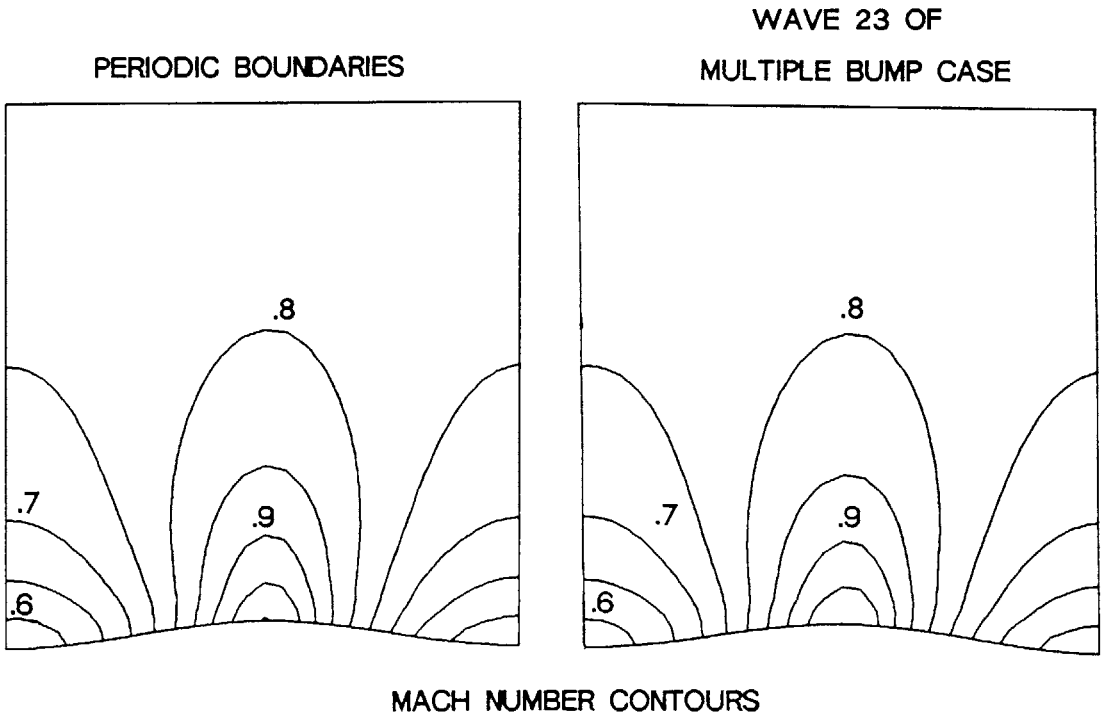

Figure 7.11: Transonic Solution Using Periodic Boundaries, $M_\infty = 0.775$, $\epsilon = 0.025$.

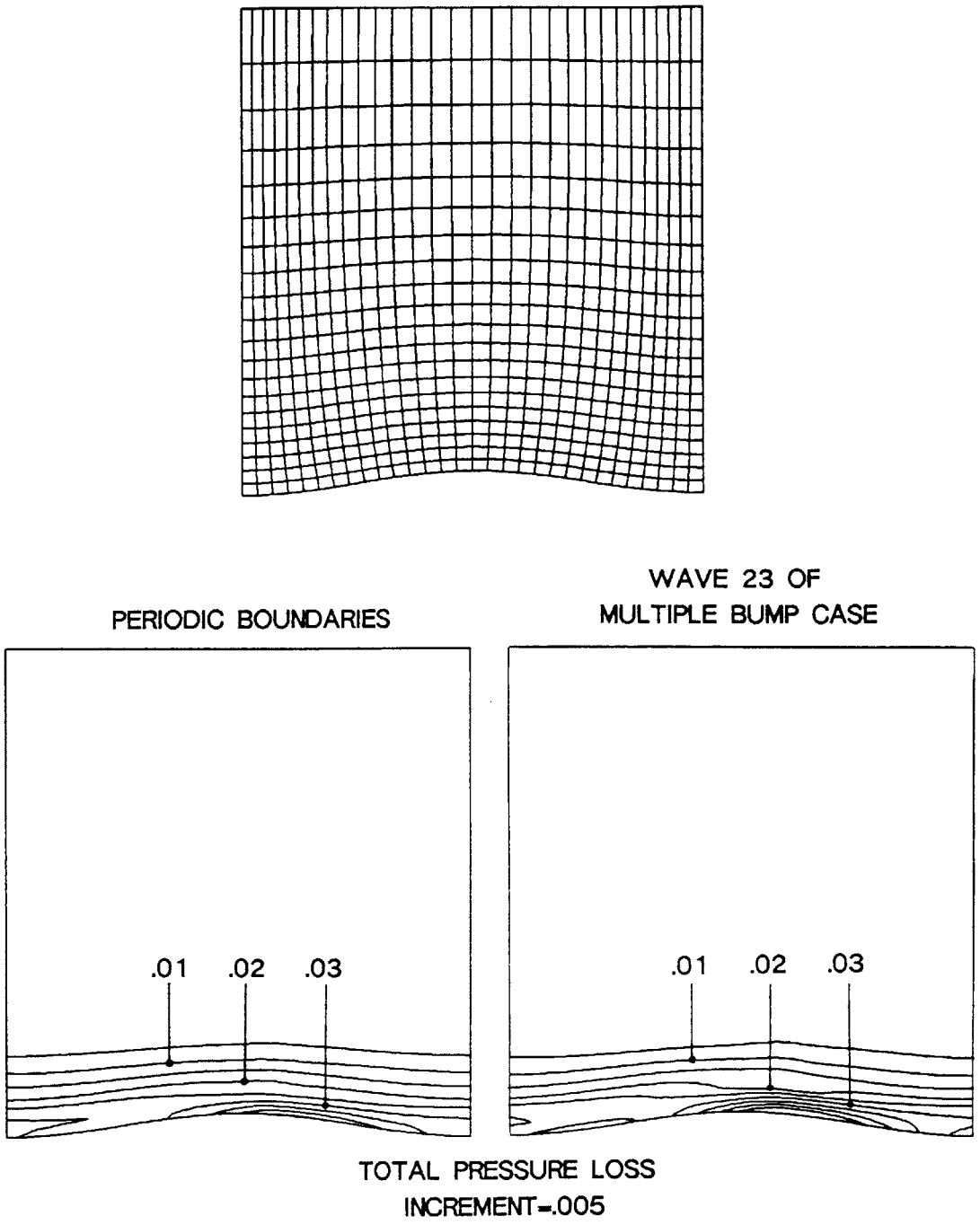

Figure 7.12: Transonic Solution Using Periodic Boundaries, $M_\infty = 0.775$, $\epsilon = 0.025$.

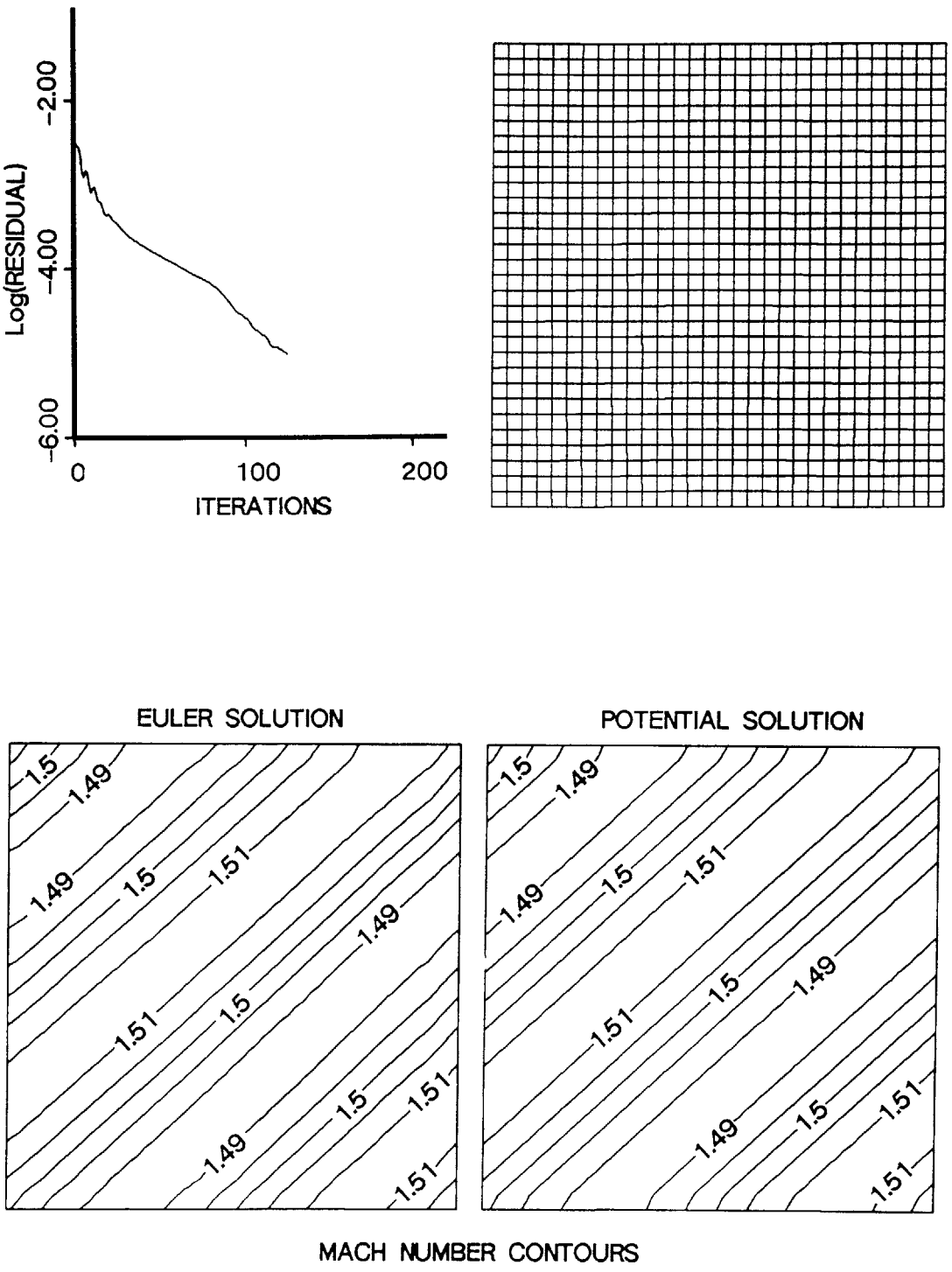

Figure 7.13: Supersonic Solution Using Imposed Boundaries, $M_\infty = 1.5$, $\epsilon = 0.001$.

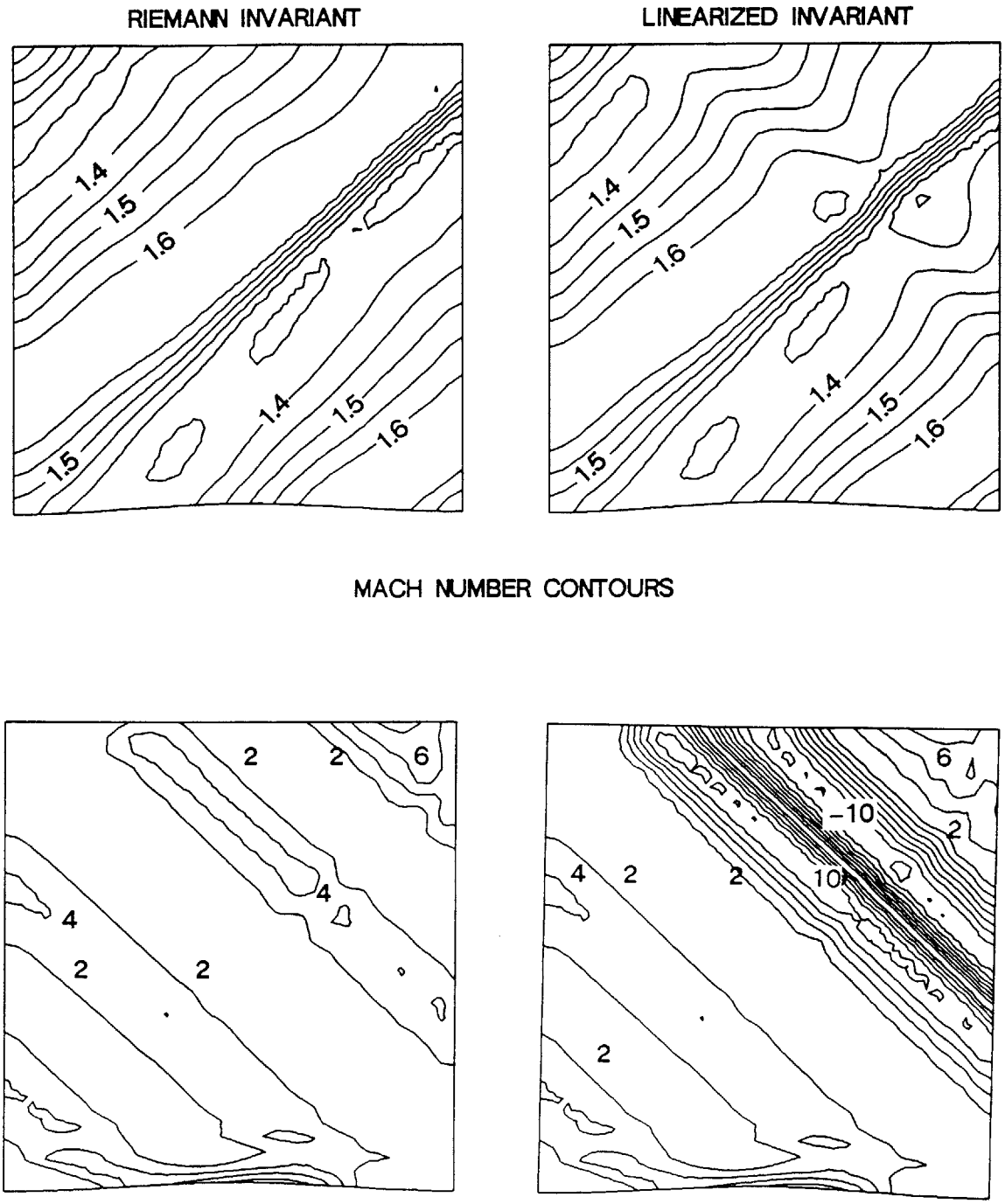

Figure 7.14: Supersonic Solution Using Imposed Boundaries, $M_\infty = 1.5$, $\epsilon = 0.01$.

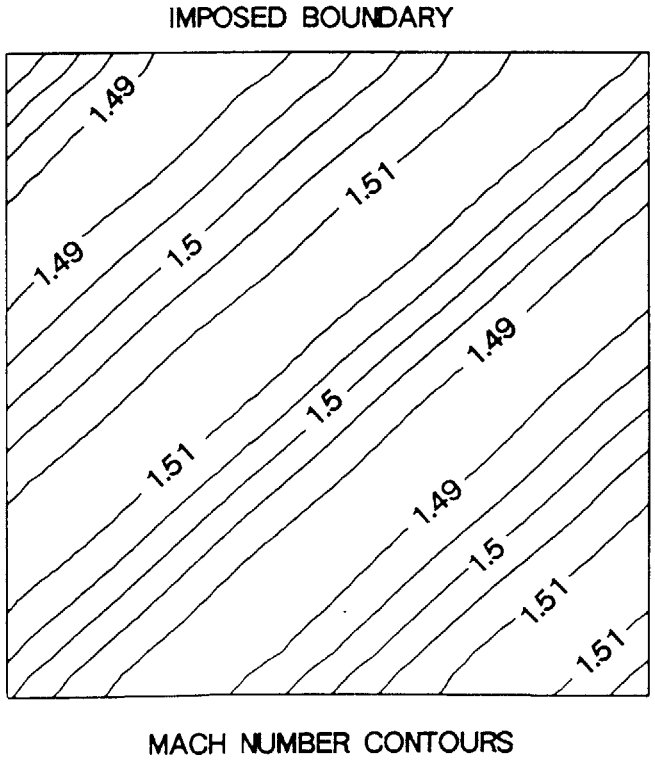

Figure 7.15: Supersonic Solution Using Periodic Boundaries with Imposed Top Boundary, $M_\infty = 1.5$, $\epsilon = 0.001$.

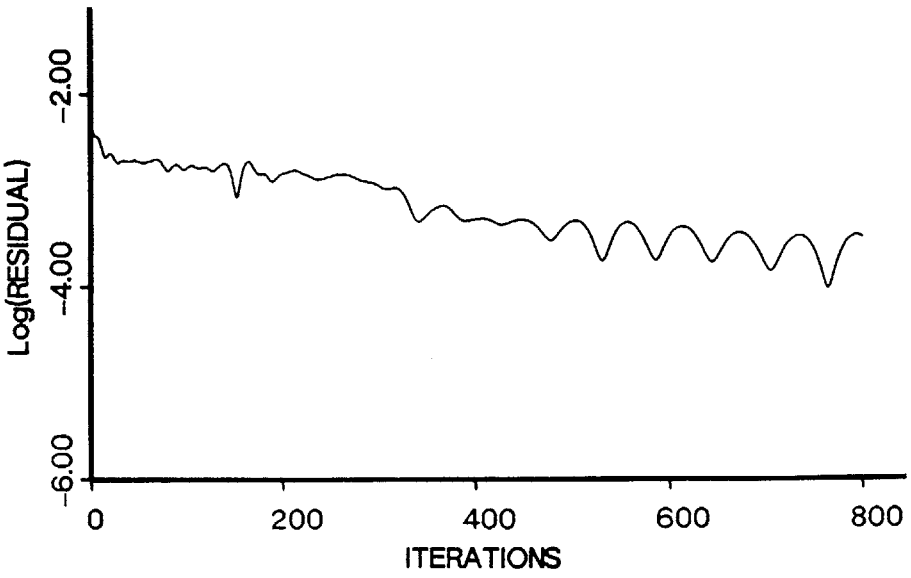

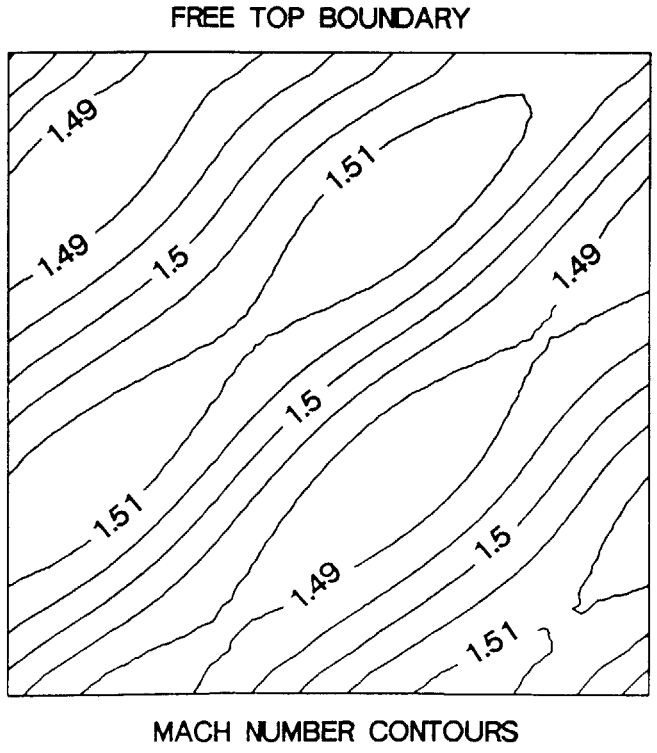

Figure 7.16: Supersonic Solution Using Periodic Boundaries with Free Top Boundary, $M_\infty = 1.5$, $\epsilon = 0.001$.

Chapter 8

CONCLUSIONS

A number of computations of the Euler flow past a wavy wall have been obtained. In so doing, an investigation of the differences between the linearized invariant boundary conditions with a modified outflow specification and the Riemann invariant boundary conditions was performed. It is concluded that in general the Riemann invariant boundary conditions are superior. While the Riemann conditions will reflect entropy waves, these tend to settle down faster than the pressure waves reflected by the linearized condition. This results in a faster convergence time and the ability to do time accurate computations provided that no total pressure loss is convected into an outflow boundary. Based on this conclusion, a series of solutions to the wavy wall problem were performed for subsonic, transonic and supersonic flow using the Riemann invariant boundary conditions in conjunction with three problem formulations.

Solutions for the subsonic Euler flow past a wavy wall were attempted by imposing the potential solution, by assuming periodicity in the flow direction, and by arranging a series of waves along a flat wall. It was found that regardles of the formulation the Euler flow past a wavy wall is periodic. The imposed potential solution resulted in the least amount of computational effort while the multiple wave solution resulted in the

largest effort.

The transonic solutions were obtained by the multiple wave formulation and by enforcing periodicity in the flow direction. For this regime the Euler computations predict that the flow starts out as a series of decreasing strength shocks. This results in an aggregate total presure loss within the solution. The flow eventually becomes periodic in space with a sonic point located at the top of each wave crest.

Based on the subsonic and transonic solutions it was concluded that the Euler flow past a wavy wall does result in a periodic solution for some flows. In addition, boundary conditions which are periodic in the flow direction can be used and provided good flexibility for a moderate cost.

The supersonic results were not periodic as expected and additional investigations were performed. By examining two different wave heights it was found that both the Riemann invariant and linearized invariant boundary conditions are not generally applicable to the problem under consideration. Both boundary conditions were found to be reflective in the outflow region unless the correct supersonic characteristics were implied by the far field values being used.

Bibliography

[1] Liepman, H.W. and Roshko, A. : Elements of Gasdynamics, John Wiley & Sons Inc., New York, (1957).

[2] Shapiro, A.H. : The Dynamics and Thermodynamics of Compressible Fluid Flow, The Ronald Press Company, New York, (1953).

[3] Chang, K. and Kwon, O.J. : Mixed Transonic Flow over a Wavy Wall with Emdedded Shock Waves, Trans. Jap. Soc. Aero. & Space Sciences, Vol. 25, No 70, pp. 189-202, (1983).

[4] Murman, E.M. and Cole, J.D. : Calculation of Plane Steady Transonic Flows, *AIAA Journal*, Vol. 9, No. 1, pp. 114-121, (1971).

[5] Krupp, J.A. : The Numerical Calculation of Plane Steady Transonic Flows Past Thin Lifting Airfoils, Ph. D. Dissertation, University of Washington, (1971).

[6] Krupp, J.A. and Murman E.M. : Computation of Transonic Flows Past Lifting Airfoils and Slender Bodies, *AIAA Journal*, Vol. 10, No. 7, pp. 880-886, (1972).

[7] Murman, E.M. : Analysis of Embedded Shock Waves Calculated by Relaxation Methods, *AIAA Journal*, Vol. 12, No. 5, pp. 626-632, (1974).

[8] Murman, E.M., Bailey, F.R., Johnson, M.L. : TSFOIL-A Computer Code for 2-D Transonic Calculations, Including Wind-Tunnel Wall Effects and Wave-Drag Evaluation, NASA SP–347, Part II, pp. 769-788, (1975).

[9] Jameson, A., Schmidt, W., and Turkel, E. : Numerical Solution of the Euler Equations by Finite Volume Methods Using Runge–Kutta Time–Stepping Schemes, AIAA Paper 81-1259, June (1981).

[10] Ni, R. : A Multiple-Grid Scheme for Solving the Euler Equations, *AIAA Journal*, Vol. 20, No. 11, pp. 1565-1571, November, (1982).

[11] Rizzi, A.W., and Erickson, L.E., : Computation of Flow Around Wings Based on the Euler Equations, *Journal of Fluid Mechanics*, November, (1984).

[12] Lax, P.D., and Wendroff, B., : Systems of Conservation Laws, *Communications in Pure and Applied Mathematics*, Vol. 30, pp. 117-130, (1951).

[13] Eriksson, L.E., : Boundary Conditions for Artificial Dissipation Operators, Aeronautical Reasearch Institute of Sweeden, FFA TN 1984-53, October (1984).

[14] Enquist, B., and Majda A. : Absorbing Boundary Conditions for the Numerical Simulation of Waves, *Mathematics of Computations*, Vol. 6, pp. 207-216, (1972).

[15] Allmaras, S.R. : Embedded Mesh Solutions of the 2–D Euler Equations Using a Cell–Centered Finite Volume Scheme, MIT Report CFDL-TR-85-4, August (1985).

[16] Usab, W.J. : Embedded Mesh Solution of the Euler Equation Using a Multiple–Grid Method, Ph.D. Thesis, Department of Aeronautics and Astronautics, MIT, January, (1984).

[17] McCartin, B.J. : Theory, Computation, and Application of Exponential Splines, Ph.D. Thesis, Department of Mathematics, New York University, October, (1981).

[18] Moretti, G. : The λ–Scheme, *Computers and Fluids*, Vol. 7, pp. 191-205, September (1979).

[19] Zannetti, L. and Colasurdo, G. : Unsteady Compressible Flow: A Computational Method Consistent with Physical Phenomena, AIAA–Paper 81-4174, July (1981).

[20] Giles, M. : Professor of Aeronautics and Astronautics, Massachusetts Institute of Technology, *Private Communication* , December (1985).

[21] Murman, E. : Professor of Aeronautics and Astronautics, Massachusetts Institute of Technology, *Private Communication* , November (1985).

[22] Giles, M. : Eigenmode Analysis of Unsteady One–Dimensional Euler Equations, NASA Contractor Report 172217, August (1983).